THE ASTRONOMICAL JOURNAL VOLUME 101, NUMBER 6 JUNE 1991

H I CONTENT AND FIR EMISSION OF S0 GALAXIES

PAUL B. ESKRIDGE[1]
Physics Department, Rensselaer Polytechnic Institute, Troy, New York 12180
and
Dudley Observatory, 69 Union Avenue, Schenectady, New York 12308

RICHARD W. POGGE
Department of Astronomy, The Ohio State University, 174 West 18th Avenue, Columbus, Ohio 43210
Received 5 July 1990; revised 25 February 1991

ABSTRACT

We have examined the relationship between H I content and FIR emission of a sample of 252 S0 galaxies. Using statistical methods that take limit values into account (survival analysis), we evaluate a best-fit linear regression line for the logarithms of the H I content versus the FIR emission (both scaled by the blue flux) with a slope of roughly unity. This slope is not significantly different for subsets of barred versus unbarred galaxies; however, the slopes differ for S0 and SB0 galaxies (the "S0 sample") versus S0/*a* and SB0/*a* galaxies (the "S0/*a* sample") at the 96% confidence level. Applying the Kaplan–Meier estimator and a battery of two-sample tests, we find that the presence or absence of bars does not affect either the relative H I content or FIR emission in our sample. These tests do show the S0/*a* sample to have relatively more H I and stronger FIR emission than the S0 sample. The presence or absence of bars, and the differences between S0 and S0/*a* systems do not significantly affect the distribution of the 60–100 μm flux ratio ($r_{60/100}$). Roughly 34% of our sample has $r_{60/100} \geqslant 0.447$, the critical value of Helou above which a majority of the FIR emission is expected to be due to star formation. Repeating these analyses on a sample from which all systems with known nuclear emission have been removed does not yield significantly different results. However, among the subset of known AGN, the relative FIR emission and relative H I content are greater than for the normal S0 galaxies to many σ. Our results indicate that, by and large, S0 galaxies have a normal ISM, at least for those components probed by the H I line and satellite FIR. Where there are glaring exceptions to this, comparison with other observations indicates that those systems with relatively more H I than expected on the basis of their FIR emission appear to have accreted their H I gas. Those systems with excess FIR emission for their H I content may be examples of galaxies that have been swept of their H I gas, or that are currently undergoing bursts of enhanced star formation.

1. INTRODUCTION

The S0 galaxies are a class first postulated by Hubble (1936) to serve as a transition between the nominally one-component elliptical (*E*) galaxies and the bulge/disk composite spiral galaxies. As such they were supposed to possess disks, and exhibit large bulge to disk (*B*/*D*) ratios, but not exhibit spiral structure. Also, they were expected to have very little interstellar material or on-going star formation. The S0 class was observationally realized some while later (see Sandage 1961), and seemed to basically obey the above precepts. The standard picture of S0's that arose was that of inert, gas-free, population II disk galaxies.

This picture has begun to unravel with the detection of clear signatures of interstellar material and star formation in many S0 galaxies [see, e.g., Wardle & Knapp 1986 for H I work; Pogge & Eskridge 1987 for Hα; Thronson *et al.* 1989 for CO; Knapp *et al.* 1989 hereafter referred to as (KGKJ) for FIR]. The physical relationship between these different components of the interstellar medium (ISM) of S0 galaxies is a key question in understanding the mechanisms by which gas is supplied to and removed from early type galaxies.

This paper addresses the relationship between H I and FIR emission from S0's. Although it is expected that the bulk of the FIR emission will originate from dust associated with molecular, rather than atomic gas (but see Jackson *et al.* 1991), the current body of data on molecular gas in S0 galaxies is too small to provide a good statistical sample. The only quantitative signatures of interstellar material for which a large number of systems have been examined are H I content and FIR emission. All the data for this study have been obtained from the literature. The sample construction is discussed in Sec. 2. Section 3 presents our statistical analysis. Because of the significant fraction of nondetections in our sample, the use of standard statistical methods is manifestly invalid. Instead, statistical methods, developed principally for actuarial studies, which explicitly account for upper and lower limit points ("censored" points) are applied. In Sec. 4 we discuss possible interpretations of the results obtained in Sec. 3, and note a number of individual objects with particularly interesting properties. Section 5 provides a summary of the work, along with suggestions for further observational study.

2. SAMPLE CONSTRUCTION

The data for this study were taken entirely from the literature. In any study comparing two observational quantities, it is desirable to have as homogeneous a set of observations as is possible. As the FIR data are entirely from the *IRAS* survey, heterogeneity is not a serious concern. The H I data, however, have been obtained with a number of different telesco-

[1] Current address: Department of Astronomy, David Rittenhouse Lab, University of Pennsylvania, Philadelphia, PA 19104.

 0004-6256/91/062056-22$00.90

pe/receiver combinations with a wide range of flux limits, and are thus rather heterogeneous. The properties of these data warrant discussion before proceeding.

2.1 The H I Data Sample

The majority of the H I data were taken from the compilation of Wardle & Knapp (1986). Additional data have been obtained from a number of other sources (see notes to Table 1). Because of the large range of sensitivity of the various telescope/receiver combinations, the intrinsic quality of the data (the smallest detectable signal) varies over several orders of magnitude: the range in observational rms noise for the detected galaxies listed in Wardle and Knapp is 0.1 mJy $< \sigma <$ 100 mJy. This is clearly a matter of concern, but is also unavoidable. The best that can be done is to proceed with care, bearing this problem in mind.

2.2 The FIR Data Sample

The FIR data are taken from the recent work of KGKJ, who have co-added raw *IRAS* data at the positions of $\approx$1150 early type galaxies in order to improve on the sensitivity available in the original Point Source Catalog (see Lonsdale *et al.* 1985). The *IRAS* data are, in general, quite homogeneous. There are occasional problems resulting from incomplete coverage, source confusion, or Galactic cirrus, but overall the absolute noise level is fairly stable.

2.3 The Combined Dataset

The combined dataset for this study is the intersection of our H I list and the FIR list from KGKJ. It contains 254 galaxies (see Table 1). Two galaxies (NGC 676 and NGC 3413) were eliminated. NGC 676 is seen in projection with a bright ($M \approx 9.5$) foreground star, which will contaminate the FIR data. NGC 3413 is an excellent example of an irregular system masquerading as an S0 (Pogge & Eskridge 1991, in preparation). This leaves a remaining sample of 252 objects. We make no claims for the completeness of this sample in any sense. Our sample selection and intent differ significantly from those of Haynes *et al.* (1990). Their study attempted to analyze statistically complete samples of cluster versus field S0's for a relation between H I content and FIR emission. In this study, we seek to examine as large a sample of S0's as is available, with no attempt to separate field and cluster system. We do, however, examine the properties of barred versus nonbarred, and early (S0, SB0) versus late-type (S0/*a*,SB0/*a*) systems (see Sec. 3). We also examine the effects of nonthermal nuclear emission on our results by analyzing a subset of our sample from which all systems with known nuclear emission have been removed.

3. STATISTICAL ANALYSIS

3.1 Statistical Methods For Censored Data

When analyzing data which have been selected by some initial criterion and then subject to secondary criteria, typically not all objects will "survive" the secondary criteria. The dataset will thus be censored in the sense that it will possess upper or lower limits. In the case we consider here the primary criterion was to select galaxies classified as S0 or S0/*a* on the basis of their optical morphology on survey plates. This sample was then subject to observations in the H I 21 cm line and the *IRAS* FIR bands. For a substantial fraction of the primary sample the secondary criteria yield only upper limits. Traditionally, astronomers have either treated limit values as detections at that value, or ignored the limit points. The first method is clearly inappropriate. The second is both wasteful, and can lead to spurious results. Usual statistical methods are not valid tools for addressing such data. Instead, methods that explicitly and consistently include the effects of limit values must be employed. Such methods belong to a field generally called "survival analysis" developed originally for actuarial studies. All of our analysis of the H I and FIR data for our sample of S0 galaxies will use techniques which are presented and discussed in detail in Schmitt (1985), Feigelson & Nelson (1985), and Isobe *et al.* (1986). The reader who wishes to see a more complete discussion of these methods and their application to astronomical data should refer to those papers.

3.2 The Relationship of H I Content to FIR Emission

3.2.1 The full dataset

For each system, the quoted 21 cm flux integral, or 3σ upper limit was taken from Table 1, and converted to a true observed flux. This quantity was then scaled by the true apparent blue flux, derived from B_T^0 as defined by de Vaucouleurs *et al.* (1976) (RC2), to give a measure of the relative strength of the H I emission per unit optical emission. While *H*-band fluxes would be far preferable to *B*-band fluxes, most of our sample do not have integrated *H*-band data available (see also Haynes *et al.* 1990 for an alternate method of normalization). It is clear that some form of normalization is needed, as otherwise all one will actually test is whether an object that is bright in one band is also bright in another, rather than the extent to which the relative strength per unit stellar content between the two quantities is related.

The FIR data were reduced in a similar way. First the 60 μm and 100 μm flux integrals (or the 3σ upper limits) were taken from KGKJ and the quantity FIR was evaluated (following Lonsdale *et al.* (1985):

$$\mathrm{FIR} = 1.26\times 10^{-14}[2.58 f_\nu(60) + f_\nu(100)]. \qquad (1)$$

This quantity was then scaled by the true apparent blue flux. Note that, for this analysis, if a given object was undetected in either the 60 or 100 μm band, the value of FIR is taken to be an upper limit.

Whenever one wishes to perform a regression between two quantities, it must first be determined that the two are statistically correlated. In the case of doubly censored datasets (i.e., limits in both variables), the only correlation test currently available is the modified Kendall's τ test (Isobe *et al.* 1986). This test gives that the probability that the relative H I content and FIR emission in our sample are uncorrelated is $P < 10^{-4}$. It must be stressed that this is a test for *statistical*, and not physical correlation.

Given this encouraging result, we then perform a linear regression on $\log(f_{\mathrm{H\,I}}/f_B)$ vs $\log(f_{\mathrm{FIR}}/f_B)$ using the method described by Schmitt (1985). This is currently the only available regression method for doubly censored datasets. The resulting regression equation is

$$\log(f_{\mathrm{FIR}}/f_B) = 0.90(\pm 0.12)\log(f_{\mathrm{H\,I}}/f_B) + 7.38(\pm 0.83). \qquad (2)$$

This result, along with the full dataset, is shown in Fig. 1. Unfortunately, the only means of assessing errors using Schmitt's regression is via the bootstrap method outlined in his paper. Clearly, this is much less desirable than a direct

TABLE 1. H I and *IRAS* data S0 galaxies.

Name	B_T^0 [a]	21cm flux	$3\sigma_{HI}$	Notes[b]	Type[c]	12μm flux	σ_{12}	25μm flux	σ_{25}	60μm flux	σ_{60}	100μm flux	σ_{100}
		Jykm/sec	Jykm/sec			Jy	mJy	Jy	mJy	Jy	mJy	Jy	mJy
NGC 16	12.61	0	1.30	CBF	0B	0	46	0	27	0	29	0	76
NGC 80	12.75	0	5.57	CBF	0	0	27	0	35	0	53	0	240
NGC 128	12.36	0	2.59	CBF,d	0p	0	42	0.22	61	0.75	41	1.55	115
NGC 148	12.79	10.70	4.56	WK	0	0	23	0	47	0	54	0	140
NGC 160	13.06	8.72	3.19	CBF	1	0	36	0	31	0.14	49	0.58	72
NGC 254	12.43	4.22	4.22	CBF	1	0	35	0	56	0	41	0.57	78
NGC 252	12.76	0	13.67	WK	0	0.11	31	0	43	0.43	44	1.72	99
NGC 315	11.84	0	4.00	CBF	0	0	31	0	49	0.32	52	0.36	90
NGC 379	13.26	0	3.19	CBF	0	0.06	39	0.07	49	0.31	48	1.87	88
NGC 404	10.78	49.00	3.43	WK,d,g	0	0	94	0.24	89	2.32	59	4.00	800
IC 89	12.37z	2.28	2.13	CBF	0B	0	30	0	53	1.57	41	3.52	135
NGC 467	12.63	0	4.18	CBF	0	0	34	0	54	0	52	0	190
NGC 473	12.50z	7.14	2.31	CBF,i	1	0	35	0	51	1.16	33	1.87	319
NGC 474	12.10	0	5.55	WK	1	0	33	0	54	0	27	0	88
NGC 499	12.64	0	2.30	CBF	0	0	29	0	23	0	40	0	112
NGC 507	11.76	0	5.85	WK	0	0	23	0	37	0	39	0	141
NGC 524	11.36	0	1.64	WK	0	0.23	37	0	49	0.78	34	1.82	114
NGC 632	12.94	3.30	1.67	WK	0	0.35	37	0.82	57	5.03	53	6.51	137
NGC 656	12.88	0	1.25	WK	0B	0	32	0	24	0.16	37	0.27	112
NGC 661	11.65Z	0	1.19	CBF	0	0	24	0	33	0	39	0.23	37
NGC 670	12.64	6.75	1.47	CBF	0	0.09	22	0.19	30	0.82	39	1.73	63
NGC 676	9.96	7.20	3.42	WK,k	1	0	34	0	57	0.28	48	0.71	109
UGC 1277	13.41	3.90	4.49	WK	1	0.07	19	0.15	23	0.28	43	0.98	81
NGC 679	12.81	0	4.33	WK	0	0	21	0	28	0.19	33	0.30	86
NGC 680	12.40	4.00	2.52	WK,j	0	0	28	0	37	0	51	0	94
NCG 687	12.58	0	0.94	WK	0	0	31	0	26	0	43	0	115
NGC 694	12.55	5.10	1.53	WK,i	0p	0.14	36	0.25	46	2.53	42	3.87	154
NGC 712	12.42	0	7.53	WK	0	0	24	0	27	0.19	32	0.83	93
UGC 1353	13.54	10.60	12.28	WK	0	0.04	18	0	25	0.20	27	0.45	71
NGC 714	12.44	0	3.36	WK	1	0.07	25	0	36	0.09	32	0.28	92
NGC 717	13.70	2.70	2.94	WK	1	0	33	0	33	0.30	52	0.83	176
UGC 1385	13.54	2.10	1.77	WK	1B	0.20	27	1.40	30	6.13	21	7.97	90
IC 171	12.28	0	1.85	WK	0	0.07	17	0	33	0.16	67	0.34	88
NGC 890	11.98	0	2.16	CBF	0	0	19	0.13	30	0	30	0	44
NGC 936	10.91	6.00	6.00	WK,j	0B	0	23	0	45	0	44	0	90
NGC 984	13.41	7.80	1.26	WK	0	0	24	0	45	0.14	37	0.12	106
IC 1830	12.97	30.80	80.40	WK	1B	0.15	17	0.29	21	2.49	24	3.99	76
NGC 1023	9.84	63.00	10.80	WK,j,l	0B	0.23	35	0	30	0	43	0	100
NGC 1167	12.81	11.51	3.70	CBF	0	0	30	0	37	0.12	28	0.93	133
NGC 1172	12.72	0	6.50	WK	0	0	26	0	31	0	41	0	72
NGC 1175	13.03	0	4.27	WK	0	0	24	0	26	0	37	0	126
NGC 1201	11.31	0	8.01	WK	0	0	38	0	28	0	35	0	72
NGC 1291	9.20	73.80	6.90	WK,l	1B	0.25	17	0.22	28	1.87	25	11.90	99

TABLE 1. (continued)

Name	B_T^a	21cm flux	$3\sigma_{HI}$	Notes[b]	Type[c]	12μm flux	σ_{12}	25μm flux	σ_{25}	60μm flux	σ_{60}	100μm flux	σ_{100}
		Jykm/sec	Jykm/sec			Jy	mJy	Jy	mJy	Jy	mJy	Jy	mJy
NGC 1272	12.99	0	11.10	WK	0	0	25	0	35	0	50	0	370
NGC 1297	12.34	0	29.07	WK	0	0	23	0	30	0	38	0	128
NGC 1302	11.12	20.30	3.49	WK	1	0	27	0	21	0.29	32	1.78	117
NGC 1316	9.36	0	59.74	WK	0p	0.31	39	0.27	20	3.16	30	14.20	3000
NGC 1326	11.11	29.70	10.67	WK	1B	0.44	19	0.84	21	8.50	48	13.18	41
NGC 1332	11.02	0	15.78	WK	0	0.09	17	0.10	23	0.52	27	1.61	51
NGC 1344	11.04	0	39.84	WK	0	0	27	0	21	0	43	0	128
NGC 1366	12.58	0	28.26	WK	0	0	27	0	28	0	28	0.38	54
NGC 1380	10.86	0	9.83	WK	1	0.17	34	0.07	21	1.07	43	3.06	95
NGC 1381	12.10	0	26.73	WK	0	0	17	0	20	0	24	0	63
NGC 1400	11.81	0	1.34	WK	0	0	36	0.10	23	0.76	40	2.92	129
NGC 1440	12.40	0	6.20	WK	0B	0	23	0	37	0	43	1.15	88
NGC 1461	12.45	0	5.87	WK	0	0	17	0	28	0.08	24	0.28	92
IC 2006	12.03	3.00	0.50	SVS	0	0	15	0	14	0.12	15	0.28	41
NGC 1527	11.43	0	23.22	WK	0	0	31	0	28	0	45	0	90
NGC 1533	11.42	87.50	85.92	WK	0B	0	31	0.06	21	0.33	24	1.24	87
NGC 1543	11.18	0	43.39	WK	0B	0.08	15	0	25	0	28	1.43	304
NGC 1553	10.11	0	37.53	WK,e	0p	0.17	16	0.13	26	0.57	24	1.01	51
NGC 1596	11.71	15.70	27.90	WK	0	0	20	0	18	0	34	0	65
NGC 1819	11.75	2.80	2.90	WK,g	0B	0.32	26	0.79	28	7.36	33	12.25	87
UGC 3426	12.12	9.50	10.20	WK	0	0.72	33	2.97	21	4.39	71	3.11	185
NGC 2217	11.08	24.80	6.12	WK	1B	0.14	27	0.12	22	1.36	33	5.33	65
NGC 2310	11.90	0	34.16	WK	0	0	18	0	16	0.13	28	0.36	168
NGC 2300	11.50	0	11.74	WK	0	0.09	18	0	28	0	25	0	81
NGC 2554	12.84	1.40	4.05	WK	1	0.09	26	0	43	0.56	33	2.24	115
NGC 2549	11.83	0	5.20	BC	0	0	20	0	28	0.26	49	0.33	116
NGC 2562	13.47	0	2.15	CBF	0	0	31	0	47	0.17	51	0.36	161
NGC 2563	12.92	0	1.16	CBF	0	0	18	0	54	0	27	0	187
NGC 2577	12.37	0	0.80	GKS	0	0.16	28	0	50	0.16	37	1.11	171
NGC 2646	12.54	0	11.87	WK	0B	0	17	0	19	0.21	30	0.76	81
NGC 2655	10.49	33.10	3.60	H82	1	0.18	25	0.26	26	1.73	29	7.20	320
NGC 2685	11.64	32.30	5.22	WK,h,l	0p	0.10	31	0	37	0.37	42	1.66	100
NGC 2765	12.68	0	0.81	WK	0	0	25	0	39	0	32	0	149
NGC 2732	12.41	0	14.87	WK	0	0.11	18	0	19	0	23	0	66
NGC 2768	10.69	0	8.46	WK	0	0.08	27	0.10	20	0.40	31	1.22	56
NGC 2784	10.68	0	5.20	BC	0	0.15	21	0.18	26	0.33	90	4.04	450
NGC 2787	11.47	15.30	6.88	WK,l	0B	0.08	38	0.09	23	0.62	52	1.05	184
NGC 2855	12.09	0	5.45	CBF	1	0.12	18	0	28	0.57	27	2.27	66
NGC 2859	11.54	7.58	5.51	CBF,d	0B	0	28	0	36	0.32	31	0.83	72
NGC 2880	12.31	0	3.70	WK	0B	0	18	0	16	0.10	25	0.34	66
NGC 2902	13.05	7.10	4.50	WK	0	0.09	24	0	37	0.16	41	1.09	194
NGC 2911	12.32	5.61	1.27	CBF,e	0p	0	28	0	36	0.29	28	0.56	79
NGC 2962	12.52	10.26	2.49	CBF	0B	0.09	32	0	48	0.23	39	0.70	99
NGC 2950	11.54	0	3.20	WK	0B	0	17	0.11	22	0.16	33	0.18	102

TABLE 1. (continued)

Name	B_T^0 [a]	21cm flux	$3\sigma_{HI}$	Notes[b]	Type[c]	12μm flux	σ_{12}	25μm flux	σ_{25}	60μm flux	σ_{60}	100μm flux	σ_{100}
		Jykm/sec	Jykm/sec			Jy	mJy	Jy	mJy	Jy	mJy	Jy	mJy
NGC 3032	12.32	5.98	4.62	CBF,g	0	0.25	24	0.26	30	1.99	31	4.18	79
NGC 3098	12.63	0	0.70	WK	0	0.12	21	0	47	0	35	0	137
NGC 3115	9.71	0	3.64	WK	0	0.34	38	0	37	0	43	0	100
NGC 3156	12.81	0	0.77	WK	0	0	31	0	57	0.19	33	0.54	66
NGC 3166	11.07	39.20	2.40	H82	1	0.31	25	0.42	57	5.90	33	13.57	100
NGC 3203	12.40	0	47.82	WK	0	0	21	0	23	0	41	0	197
NGC 3245	11.47	0	0.70	GKS,f	0	0.15	40	0.22	40	2.09	40	3.53	75
NGC 3300	13.06	0	1.01	CBF	0B	0	42	0	56	0	25	0	90
IC 2597	12.47	0	5.39	WK	0	0.30	24	0.21	40	0.64	30	1.85	96
NGC 3384	10.50	0	0.96	WK	0B	0.18	28	0	56	0	39	0.40	75
NGC 3414	11.53	3.48	3.48	CBF,m	0	0.08	34	0	39	0.26	25	0.50	164
NGC 3413	12.47z	15.35	1.04	CBF,h	1	0.06	25	0.21	33	1.19	44	3.76	1057
NGC 3419	12.87	2.10	0.94	BB	0	0	43	0	117	0.63	33	0	213
NGC 3516	12.05	0	2.50	WK	0B	0.39	18	0.94	14	1.90	29	1.89	197
NGC 3593	11.24	10.49	1.69	CBF,g,o	1	1.31	44	2.09	57	18.87	34	35.60	59
NGC 3630	12.43	0	0.91	WK	0	0	34	0	39	0	57	0	94
NGC 3665	11.53	0	34.38	WK	0	0.10	26	0.20	26	1.96	40	6.69	163
NGC 3716	13.51	2.00	4.12	WK	0?	0	29	0	43	0.13	53	0.43	147
UGC 6527	13.79	2.00	2.91	WK	1p	0.13	21	0.24	52	0.79	33	1.94	99
NGC 3768	12.32	0	2.04	WK	0	0	32	0	41	0	34	0	279
NGC 3773	12.88	4.13	2.23	CBF,l	0p	0	30	0.17	34	1.43	39	2.24	53
NGC 3801	12.68	5.26	2.03	CBF	0	0.08	28	0.14	45	0.17	53	2.49	78
IC 719	12.17	3.30	2.25	WK,n	0?	0.23	33	0	67	0.89	52	2.36	271
NGC 3816	12.12	0	7.63	WK	0	0	36	0	37	0	37	0	67
NGC 3900	11.84	17.60	4.00	H82,l	1	0.10	27	0	32	0.40	38	1.75	167
NGC 3945	11.23	3.90	8.16	WK	0B	0.15	19	0	23	0.27	27	1.21	80
NGC 3998	11.03	6.40	3.48	WK,l,m	0	0.13	23	0.12	21	0.57	27	1.02	110
NGC 4008	12.67	0	4.42	WK	0	0	31	0	32	0.13	27	0.11	111
NGC 4026	11.25	0	4.44	WK,l	0	0.13	21	0	21	0.10	27	0.50	112
NGC 4036	11.29	0	11.90	H82	0	0.11	55	0	25	0.58	48	1.45	129
NGC 4078	12.66	0	0.75	WK	0?	0	28	0	53	0.07	29	0.46	78
NGC 4105/6	10.85	11.70	11.40	WK,p	0	0	30	0	45	0.50	46	1.37	202
NGC 4124	12.13	0	0.66	WK	0	0	28	0	48	0.44	42	1.56	63
NGC 4150	12.21	0	0.27	BB	0	0	22	0	28	1.25	37	2.37	54
NGC 4179	11.61	0	1.85	WK	0	0	63	0	48	0	31	0	57
NGC 4203	11.41	27.20	4.50	WK,e,l,m	0	0	39	0.17	26	0.61	30	1.92	71
NGC 4215	12.00	0	1.49	WK	0	0	35	0	26	0	31	0	92
NGC 4233	12.74	0	0.83	WK	0	0	42	0	57	0.20	38	0.43	77
NGC 4251	11.41	0	0.90	WK	0	0	32	0	42	0.12	39	0	80
NGC 4262	12.17	10.60	2.67	WK,l	0B	0.12	22	0	42	0.19	35	0.35	110
NGC 4267	11.57	0	1.18	WK	0B	0	26	0	40	0.19	35	1.03	36
NGC 4270	12.93	0	4.35	CBF	0	0	47	0	53	0	42	0	83
NGC 4281	12.20	0	6.30	CBF,d,n	0	0.22	33	0	47	0.63	33	1.78	90
NGC 4293	10.77	0	3.50	CBF	1	0.23	32	0.60	51	3.97	43	6.86	79

TABLE 1. (continued)

Name	B_T^o [a]	21cm flux	$3\sigma_{HI}$	Notes[b]	Type[c]	12μm flux	σ_{12}	25μm flux	σ_{25}	60μm flux	σ_{60}	100μm flux	σ_{100}
		Jykm/sec	Jykm/sec			Jy	mJy	Jy	mJy	Jy	mJy	Jy	mJy
NGC 4308	13.29	0	0.23	WK	0	0	35	0	35	0	33	0	140
NGC 4310	12.86z	2.13	1.30	CBF,n	0	0.11	48	0	51	0.90	38	2.60	92
NGC 4324	11.79z	11.08	11.08	CBF	0	0	33	0	55	0.42	43	1.77	45
NGC 4340	11.73	0	0.87	WK	0B	0	24	0.31	51	0.09	25	0.33	55
NGC 4342	13.33	0	1.00	WK	0	0	43	0	47	0	66	0	160
NGC 4344	12.34	2.34	1.66	CBF	0?	0.08	31	0.10	30	0.47	42	1.58	63
NGC 4350	11.67	0	0.89	WK	0	0.14	43	0	37	0.37	35	0.97	74
NGC 4352	13.32	0	0.69	WK	0	0	30	0	51	0	32	0	96
NGC 4371	11.69	0	1.01	WK	0B	0	26	0	45	0	48	0	139
NGC 4377	12.46	0	0.90	WK	0	0	25	0	44	0.37	52	0.98	122
NGC 4379	12.09	0	1.12	WK	0	0	28	0	37	0	47	0	112
NGC 4382	9.90	0	1.52	WK	0p	0	40	0.46	28	0.15	30	0	67
NGC 4385	12.69	4.68	3.74	CBF,i	0B	0.27	47	1.15	66	4.55	30	5.91	92
NGC 4417	11.86	0	0.96	WK	0	0	30	0	77	0	44	0	106
NGC 4421	12.24	0	1.28	WK	1B	0	38	0	38	0	43	0	58
NGC 4425	12.57	0	0.68	WK	1B	0	33	0	49	0	60	0	146
NGC 4429	10.93	0	1.43	WK,n	0	0.20	31	0	40	1.60	45	4.58	95
NGC 4441	12.93	0	14.26	WK	0p	0.13	21	0.51	27	2.96	30	4.04	82
NGC 4435	11.52	0	0.93	WK,d,n	0B	0.12	45	0.21	50	2.05	44	4.16	106:
NGC 4442	11.10	0	1.21	WK	0B	0	35	0	46	0.13	43	0.25	89
NGC 4451	13.09	3.36	1.19	CBF,n	0	0.17	35	0.40	46	1.75	39	4.60	88
NGC 4452	13.10	0	1.30	CBF	0	0	28	0	40	0	33	0	85
NGC 4457	11.38	7.40	3.33	CBF,g	1	0.31	44	0.57	57	4.85	37	9.38	68
NGC 4459	11.28	0	4.31	CBF,d,g,n	0	0.33	27	0	90	1.92	67	4.28	119
NGC 4464	13.38	0	0.68	WK	1	0	44	0	47	0	31	0.31	75
IC 796	12.65	0.60	1.80	WK	1	0.08	29	0	43	0.61	37	1.40	101
NGC 4470	12.37	8.40	3.78	CBF	1	0.14	33	0.19	40	1.91	48	3.88	157
NGC 4474	12.49	0	1.19	WK	0	0	37	0	42	0	48	0	80
NGC 4476	12.93	0	0.78	WK	0	0	47	0	40	0.68	38	1.64	96
NGC 4477	11.03	0	1.08	WK	0B	0.16	34	0	44	0.59	52	1.25	87
NGC 4479	13.08	0	0.71	WK	0B	0	33	0	52	0	25	0	134
NGC 4483	13.20	0	0.64	WK	0B	0.08	28	0	51	0	37	0.42	147
NGC 4488	13.59	0	0.71	WK	1B	0	58	0	45	0.15	41	0.20	103
NGC 4497	13.08	0	0.66	WK	0	0	33	0	43	0	20	0	307
NGC 4503	12.06	0	1.47	CBF	0B	0	25	0	28	0	40	0	169
NGC 4515	12.81	0	0.63	WK	0	0	35	0.10	54	0	34	0.92	73
NGC 4526	10.38	0	0.94	WK,f,h	0	0.44	39	0.53	49	5.72	47	21.00	270
NGC 4528	12.43	0	0.81	WK	0	0	35	0	55	0	42	0	133
NGC 4546	11.06	0	6.87	WK	1B	0	33	0.13	60	0.27	46	0.79	196
NGC 4550	12.13	0	1.66	WK	0	0	29	0	63	0.14	31	0.22	80
NGC 4544	13.44	2.90	1.25	WK	1B	0	30	0.19	65	0.99	53	2.81	141
NGC 4570	11.45	0	0.95	WK	0	0	27	0	75	0	46	0	97
NGC 4578	11.81	0	0.37	WK	0	0	40	0	38	0	34	0	98
NGC 4608	11.82	0	2.55	CBF	0B	0	22	0	57	0	25	0.21	58

TABLE 1. (continued)

Name	B_T^o [a]	21cm flux	$3\sigma_{HI}$	Notes[b]	Type[c]	12μm flux	σ_{12}	25μm flux	σ_{25}	60μm flux	σ_{60}	100μm flux	σ_{100}
		Jykm/sec	Jykm/sec			Jy	mJy	Jy	mJy	Jy	mJy	Jy	mJy
NGC 4612	11.81	0	0.97	WK	0	0	31	0	37	0	41	0	75
NGC 4620	12.81	0	0.90	WK	0	0	28	0	39	0	46	0	136
NGC 4623	12.86	0	1.33	WK	0	0	44	0	49	0	23	0	106
NGC 4638	11.78	0	1.11	WK	0	0	21	0	32	0	45	0	66
NGC 4643	11.32	4.30	1.94	CBF	1B	0	26	0	48	0.64	27	1.83	80
NGC 4659	12.82	0	0.90	WK	1	0	31	0	31	0	35	0	110
NGC 4665	11.90	0	6.10	WK	1B	0	21	0	48	0	27	0	44
NGC 4694	11.99	4.95	1.74	CBF,l	0B	0	42	0.19	48	1.27	51	2.68	154
NGC 4710	11.64	0.32	0.04	q	0	0.23	37	0.65	48	5.89	42	13.15	156
NGC 4754	11.19	0	1.32	WK	0B	0	26	0	43	0	45	0	102
NGC 4762	11.04	0	0.92	WK	0B	0.14	50	0	33	0	48	0	71
NGC 4839	12.09	0	2.14	WK	0	0	55	0	31	0	20	0	76
NGC 4856	11.13	4.40	10.91	WK	1	0	40	0	41	0.17	32	0.41	139
NGC 4866	11.41	22.16	2.27	CBF	1	0.11	44	0.22	44	0.15	52	0.91	145
NGC 4880	12.80	0	2.80	CBF	0	0	17	0	57	0	34	0	129
NGC 4914	12.06z	0	3.76	CBF	0	0	23	0.11	28	0	30	0	40
NGC 4958	11.23	0	5.89	WK	0	0.16	26	0	43	0.28	47	0.31	116
NGC 5018	11.40	0	73.14	WK	0	0.19	33	0	55	0.98	41	1.65	80
NGC 5084	11.71	96.40	129.10	WK,l	0	0	48	0	49	0.42	42	2.30	330
NGC 5087	11.70	0	8.54	WK	0	0	29	0.22	46	1.11	41	2.78	175
NGC 5101	11.27	57.26	7.92	CBF,l	1B	0.11	25	0.11	36	0.78	31	5.60	280
NGC 5102	10.23	72.00	20.97	WK,l	0	0.08	31	0.17	33	0.94	35	2.43	90
NGC 5273	12.21	0	1.22	WK	0	0.11	22	0.27	24	0.93	35	1.39	108
NGC 5291	13.07	63.00	28.35	WK	0	0	30	0	41	0	52	0	92
NGC 5308	11.92	0	30.31	WK	0	0	21	0	21	0	40	0	79
NGC 5338	13.25	0.70	0.96	WK	0B	0	35	0	53	0.42	35	0.55	100
NGC 5363	10.81	1.80	1.51	WK,e,h	0	0.19	36	0.22	50	1.70	46	4.45	45
NGC 5389	12.63	0	19.76	WK	1	0.05	21	0	13	0.42	18	1.74	64
NGC 5380	12.97	0	3.00	CBF	0	0	23	0	32	0	27	0	185
NGC 5422	12.45	0	3.57	WK	1	0	18	0	16	0.07	27	0.33	71
NGC 5424	13.16	0	11.28	WK	0	0	34	0	47	0.13	66	0.38	108:
NGC 5473	12.10	0	5.40	BC	0	0	21	0.07	25	0.09	14	0.32	60
NGC 5485	12.14	0	8.42	WK	0	0	20	0	19	0.15	34	0.85	88
NGC 5493	12.05	8.00	7.80	WK	0	0	40	0	57	0	40	0	94
NGC 5532	12.64	0	11.07	WK,e	0	0.07	27	0	34	0	38	0.48	89
NGC 5574	12.97	0	0.93	WK	0	0	36	0	33	0	40	0	447
NGC 5611	12.99	0	1.16	WK	0	0	38	0	33	0	40	0	99
NGC 5631	12.19	4.00	6.75	WK,j	1	0	22	0.11	27	0.23	34	0.92	76
NGC 5687	12.34	0	5.39	WK	0	0	20	0	15	0	20	0	45
NGC 5791	12.42	0	22.31	WK	0	0	32	0	32	0	27	0	135:
NGC 5820	12.71	6.80	4.95	WK	0	0.06	15	0	14	0.13	39	0.47	147
NGC 5838	11.42	0	2.40	CBF,e	0	0.12	28	0.09	41	0.75	40	1.48	82
NGC 5866	10.61	0	5.00	BC,g	0	0.30	16	0.24	14	5.21	21	16.61	51
NGC 5854	11.99	0	2.07	CBF	0B	0	34	0	32	0	33	0	166

TABLE 1. (continued)

Name	B_T^0 [a]	21cm flux	$3\sigma_{HI}$	Notes[b]	Type[c]	12μm flux	σ_{12}	25μm flux	σ_{25}	60μm flux	σ_{60}	100μm flux	σ_{100}
		Jykm/sec	Jykm/sec			Jy	mJy	Jy	mJy	Jy	mJy	Jy	mJy
NGC 5898	12.05	0	15.30	WK	0	0	31	0.22	59	0.13	37	0.20	64
UGC 10528	12.80	5.70	1.49	WK	0	0.10	31	0.05	17	0	21	0.15	123
NGC 6278	12.31	0.90	1.50	WK,m	0	0.05	25	0.06	23	0	23	0.28	88
NGC 6359	13.12	0	11.20	WK	0	0	17	0	13	0	15	0.28	96
NGC 6501	12.56	5.20	1.92	WK,j,l	1	0	23	0	31	0	29	0	187
NGC 6654	11.96	0	17.15	WK	1B	0	19	0	15	0.26	26	1.42	65
NGC 6684	10.71	0	27.74	WK	1B	0.12	24	0.07	29	0	47	0	93
NGC 6703	11.92	0	37.76	WK	0	0	25	0	17	0	67	0	177
NGC 6861D	11.56	0	66.56	WK	0	0	26	0.07	27	0.44	42	1.78	84
IC 5063	12.78	9.70	5.28	WK	1	1.22	22	3.99	28	6.53	32	3.92	200
NGC 7013	11.62	21.60	2.33	WK,g,i,l	1	0.11	23	0.22	23	1.98	50	4.44	133
NGC 7020	12.05	0	59.79	WK	0	0	27	0.12	23	0	38	0.20	57
NGC 7135	12.30	0	6.50	BC	0p	0	25	0	28	0.26	32	0.70	29
NGC 7180	13.08	1.38	1.38	CBF,j	0	0	24	0	39	0.12	41	0.53	89
IC 5181	12.03	0	32.23	WK	0	0	30	0	45	0.10	22	0.35	56
NGC 7252	12.35	0	8.20	BFG	0p	0.26	20	0.52	43	4.40	32	6.87	63
NGC 7280	13.22	2.70	4.65	WK,j,l	1	0	31	0	28	0.21	29	0.37	86
NGC 7302	12.60	4.00	5.82	WK	0	0	30	0	38	0.09	34	0.53	211
NGC 7332	11.31	0	1.74	WK	0	0.11	25	0	32	0.22	30	0.36	96
NGC 7377	12.28	0	11.55	BFG	1p	0	30	0	41	0.39	46	1.48	104
NGC 7457	11.44	0	0.56	WK	0	0	24	0	33	0.11	42	0.40	170
NGC 7550	12.48z	0	0.96	CBF	0	0.11	35	0	23	0.11	47	0.44	199:
NGC 7576	12.94	0	40.57	WK	0	0	44	0	70	0.43	66	0.92	152
NGC 7585	12.28	0	13.39	BFG	1	0	35	0	43	0.12	42	0.31	70
NGC 7611	13.24	0	1.59	WK	0	0	35	0	57	0	47	0	245
NGC 7617	14.43	0	3.75	WK	0	0.05	29	0	38	0.32	59	1.23	227
NGC 7623	13.13	0	1.19	CBF	0	0	44	0	49	0	57	0	180
NGC 7625	12.49	19.58	1.82	CBF,g	1	0.61	38	1.07	38	8.85	27	18.85	84
NGC 7634	13.39	0	1.29	CBF	0B	0	32	0	36	0	34	0	114
NGC 7648	13.19	0.66	0.66	CBF	0	0.16	46	0.63	44	4.92	46	7.40	85
NGC 7679	12.86	14.12	4.71	BFG	1	0.49	43	1.08	95	7.79	52	10.50	74:
NGC 7742	11.98	15.20	0.19	WK,i	1	0.19	38	0.36	37	2.87	39	6.32	132
NGC 7743	11.81	4.70	4.70	CBF,j	1B	0.09	38	0.17	28	0.95	42	3.02	191
NGC 7779	12.07	0	45.99	WK	1	0	38	0	53	0.21	64	0.85	205
UGC 12840	13.09	2.40	0.73	WK	0B	0	43	0	27	0	37	0.40	111

Notes to TABLE 1

a). Magnitudes from RC2 or WK where available. Those followed by a lower case z where computed from Zwicky magnitudes by the method given in Knapp *et al.* (1985) using extinctions from the RC2. The extinction for the one system followed by an upper case Z (NGC 661) was obtained from Burstein and Heiles (1984).

b). Following are the references for the HI data corresponding to the capital entries in column 5:
BFG: Balick, Faber, and Gallagher 1976.
BC: Balkowski and Chamaraux 1983.
BB: Bieging and Biermann 1977.
CBF: Chamaraux, Balkowski, and Fontanelli 1986.
GKS: Giovanardi, Krumm, and Salpeter 1983.
H82: Huchtmeier 1982.
SVS: Schweizer, van Gorkom, and Seitzer 1989. Includes HI map.
WK: Wardle and Knapp 1986.

Notes to TABLE 1 (continued)

c). There is some amount of disagreement as to the morphological types of a number of the galaxies listed (see Knapp *et al.* 1989). The type codes listed have the following meanings:
0 - Generally classed as S0 or earlier.
1 - Generally classed as S0/a or later.
B - Galaxy is barred
p - Galaxy has some peculiarity in its optical morphology
? - Significant disagreement, or uncertainty as to type

d). Bally and Thronson (1989) show these galaxies to follow the 60μ vs. 12.6cm relation for spirals.

e). Bally and Thronson show these galaxies to have 12.6cm excesses relative to their 60μ fluxes.

f). Bally and Thronson show these galaxies to have 60μ excesses relative to their 12.6cm fluxes.

g). Thronson *et al.* (1989) detect these galaxies in the CO ($J = 1 \rightarrow 0$) line.

h). Thronson *et al.* give upper limits for CO line emission in these galaxies.

i). Pogge and Eskridge (1987) detect and map these galaxies in Hα.

j). Pogge and Eskridge give upper limits for the Hα emission for these galaxies.

k). This galaxy (NGC 676) is superposed on a bright ($\sim$ 9.5th magnitude) star. Its optical and infrared fluxes are therefore not trustworthy.

l). These galaxies have been mapped in HI (see van Driel 1987, and references therein).

m). Walsh *et al.* (1989) show these galaxies to have 6.1cm excesses relative to their FIR fluxes.

n). Walsh *et al.* show these galaxies to have FIR excesses relative to their 6.1cm fluxes.

o). This galaxy, NGC 3593, has been mapped in Hα by Hunter *et al.* (1989).

p). The magnitude, as well as the HI and IR fluxes and errors for this interacting pair (NGC 4105/6) have been summed.

q). HI flux from Kenney *et al.* (1991).

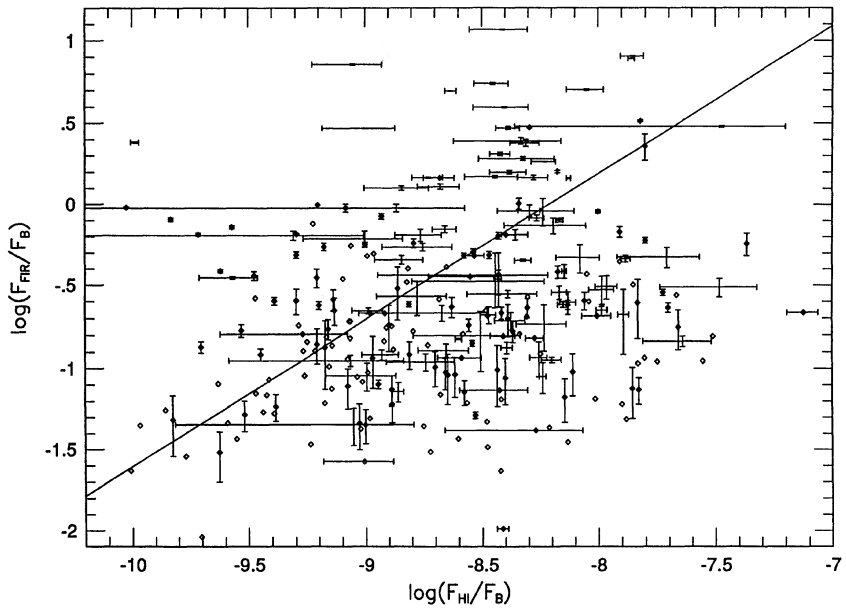

FIG. 1. $\log(F_{\rm FIR}/F_B)$ vs $\log(F_{\rm H\,I}/F_B)$ for the full set of 252 galaxies. The line is the best-fit line using Schmitt's linear regression.

means of assigning errors to the regression coefficients. There is no help for this, however. Assuming the bootstrap to give reasonable error bounds, it is clear that the two quantities are statistically related, and that the slope of the power law which is fit to them is essentially unity. There are also a number of extreme outlying galaxies which will be discussed further in Sec. 4.3 below.

3.2.2 Correction for galaxies with nuclear emission

A number of the galaxies in our sample are known to have optical nuclear spectra suggestive of nonthermal activity. These systems are listed in Table 2. Active galactic nuclei (AGN) can contribute a significant amount of the FIR flux of early type galaxies (Bally & Thronson 1989, KGKJ). We therefore repeat our analysis with a subset of the full sample from which all galaxies with known AGN are removed. This leaves a sample of 227 objects. Once again, the Kendall's τ test indicates that the probability that the H I content and FIR emission are uncorrelated is $P < 10^{-4}$. Schmitt's regression analysis gives

$$\log(f_{\rm FIR}/f_B)_{NA} = 0.88(\pm 0.12)\log(f_{\rm H\,I}/f_B)_{NA} + 7.19(\pm 0.80). \quad (3)$$

It is apparent from this that the presence or absence of systems with known nuclear emission does not significantly affect the relationship between H I content and FIR emission for this sample. However, it is possible that this is due either to the relatively small number of systems with significant nuclear emission, or to the presence of a large number of systems with as yet undetected nonthermal nuclear sources. This issue will be addressed further in Sec. 4.1 below.

TABLE 2. Galaxies with known nuclear emission.

Name	Alternate name	Type	Reference
NGC 404		Liner	[1]
IC 89	Mrk 565	Sy?	[2]
NGC 632	Mrk 1002	HII	[2]
NGC 694	Mrk 363	HII	[2]
NGC 1167		Liner	[1]
NGC 1316		Liner	[3]
NGC 1380		em	[3]
NGC 1533		Liner	[3]
NGC 1553		Liner	[3]
NGC 1819	Mrk 1194	HII	[2]
NGC 2655		Liner	[3]
NGC 2685		Liner	[3]
NGC 2768		Liner	[1]
NGC 2911		Liner	[1]
NGC 3516		Sy 1	[4]
NGC 3998		Liner	[1]
NGC 4036		Liner	[1]
NGC 4385	Mrk 52	HII	[2]
NGC 5273		Sy 1	[1]
NGC 6861d		Liner	[3]
NGC 7013		Liner	[5]
IC 5181		Liner	[3]
NGC 7679	Mrk 534	L/HII?	[5]
NGC 7742		Liner	[5]
NGC 7743		Liner	[5]

References:
[1] Huchra 1983
[2] Mazzarella and Balzano 1986
[3] Phillips *et al.* 1986
[4] Seyfert 1943
[5] Pogge, unpublished data.

3.2.3 Barred versus nonbarred galaxies

We now separate the sample into two subsets, based on the classification of the galaxies as barred or nonbarred. The classifications are taken mainly from Wardle & Knapp (1986), who attempted to apply a uniform classification criterion (see their Appendix A). This gives us 180 nonbarred and 72 barred galaxies. For each of these subsets, the Kendall's τ test indicates that the probability that the H I content and FIR emission are uncorrelated is $P < 10^{-4}$. Schmitt's method yields

$$\log(f_{\rm FIR}/f_B)_A = 0.95(\pm 0.22)\log(f_{\rm H\,I}/f_B)_A + 7.73(\pm 1.47) \quad (4a)$$

and

$$\log(f_{\rm FIR}/f_B)_B = 0.96(\pm 0.11)\log(f_{\rm H\,I}/f_B)_B + 7.96(\pm 0.78) \quad (4b)$$

for the nonbarred and barred samples, respectively. These results are plotted in Figs. 2(a) and 2(b). We conclude from these plots that the relationship between relative H I content and FIR emission is not significantly different in barred versus nonbarred S0 galaxies.

Repeating this analysis on samples with the AGN removed, we have 166 nonbarred and 61 barred galaxies. For these, the Kendall's τ test indicates that the probability that the H I content and FIR emission are uncorrelated is $P < 10^{-4}$. Schmitt's method yields

$$\log(f_{\rm FIR}/f_B)_A = 0.96(\pm 0.22)\log(f_{\rm H\,I}/f_B)_A + 7.85(\pm 1.42), \quad (5a)$$

and

$$\log(f_{\rm FIR}/f_B)_B = 1.00(\pm 0.11)\log(f_{\rm H\,I}/f_B)_B + 8.28(\pm 0.87). \quad (5b)$$

Again, there are no significant changes from the results obtained using the full dataset. The presence or absence of bars does not significantly affect the relationship between H I content and FIR emission in S0 galaxies.

3.2.4 S0 versus S0/a systems

We make a second division between galaxies classified as S0 or SB0 (referred to below as "the S0 sample") and S0/*a* or SB0/*a* (referred to below as "the S0/*a* sample"), giving totals of 199 and 53 galaxies, respectively. Again, our classifications are taken mainly from Wardle & Knapp (1986). The Kendall's τ test indicates that, for both subsamples, the probability that the H I content is uncorrelated with FIR emission is $P < 10^{-4}$. The results from applying Schmitt's method are

$$\log(f_{\rm FIR}/f_B)_0 = 0.73(\pm 0.13)\log(f_{\rm H\,I}/f_B)_0 + 5.88(\pm 0.85), \quad (6a)$$

and

$$\log(f_{\rm FIR}/f_B)_a = 1.29(\pm 0.19)\log(f_{\rm H\,I}/f_B)_a + 10.62(\pm 1.25) \quad (6b)$$

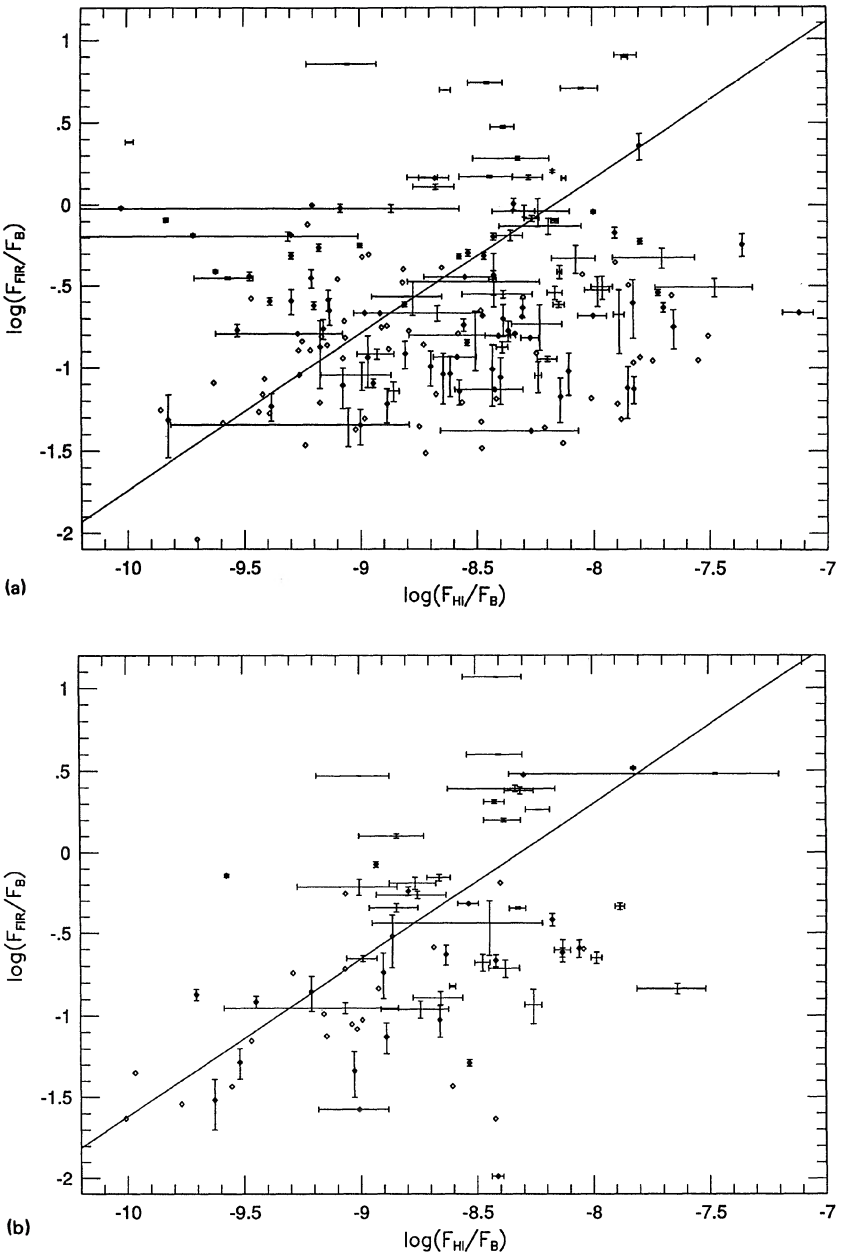

FIG. 2. Barred and nonbarred subsets of the data,with best-fit lines: (a) nonbarred galaxies; (b) barred galaxies.

for the S0 and S0/*a* samples, respectively. These results are displayed in Figs. 3(a) and 3(b). The most conservative way to consider these results is to compare the difference of the slopes with the rms of their errors. Viewed this way, and given the error estimates from the bootstrap, the slopes of the regressions differ at the 98.5% confidence level, corresponding to 2.43σ. These results indicate that the FIR emission seems to be a more steeply increasing function of the relative H I content in the S0/*a* sample than in the S0 sample.

Repeating this analysis with the AGN removed, we have 180 S0 and 47 S0/*a* galaxies. For both of these samples, the Kendall's τ test gives that the probabilities that the H I content and FIR emission are uncorrelated are $P \leqslant 3 \times 10^{-4}$. Schmitt's method yields

$$\log(f_{\rm FIR}/f_B)_0 = 0.72(\pm 0.13)\log(f_{\rm H\,I}/f_B)_0 + 5.75(\pm 0.84) \quad (7a)$$

and

$$\log(f_{\rm FIR}/f_B)_a = 1.23(\pm 0.21)\log(f_{\rm H\,I}/f_B)_a + 10.09(\pm 1.40). \quad (7b)$$

The slopes now differ at only the 96% confidence level, corresponding to 2.06σ. This weakens, but certainly does not

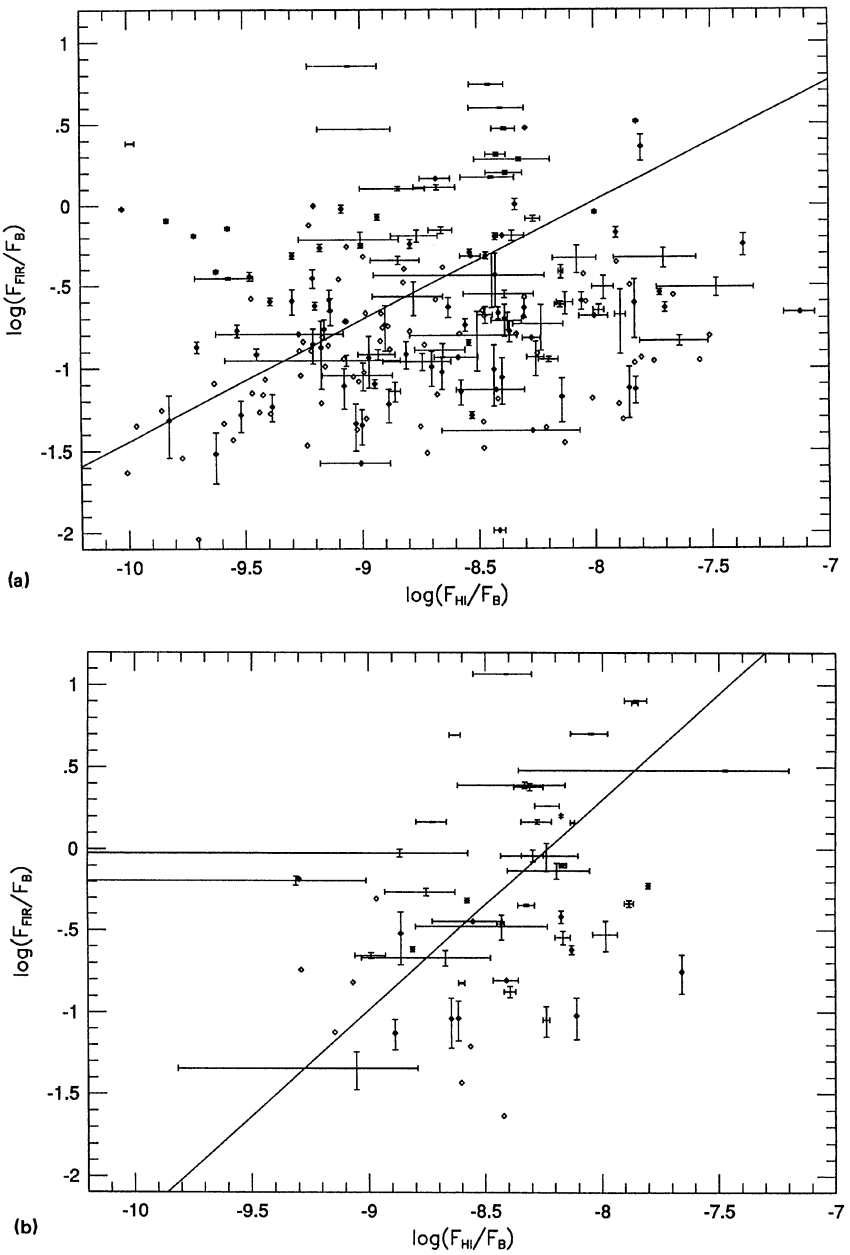

FIG. 3. S0 and S0/*a* subsets of the data, with best-fit lines: (a) S0 galaxies; (b) S0/*a* galaxies.

erase the result: there appears to be a steeper relation between H I content and FIR emission in S0/*a*'s than in S0's.

3.3 Two Sample Tests

In order to gain a more complete understanding of the distribution functions of the objects being studied, several statistical tests were made on the ensembles of H I and FIR data. The Kaplan–Meier estimator was calculated for the relative H I content, the relative FIR emission, and the 60–100 μm flux ratio ($r_{60/100}$). The Kaplan–Meier estimator is a nonparametric maximum likelihood approximation to the true distribution function underlying a data ensemble in which censoring is present. It can also be used to recover estimates of the mean and variance of the underlying distribution under regularity assumptions regarding the nature of the censoring. This test was applied to both the whole sample and the various morphological subsamples discussed above. Also, various two-sample tests were used on the mutually exclusive subsamples to examine the extent to which the morphological discriminants are connected to the H I content and the FIR emission. These tests evaluate the probability that two samples are drawn from the same underlying parent distribution. The detections and limit points are weighted in different manners for each test, thus the performance of the tests depends in different ways on the underlying form of the distributions and on the nature of the censoring. Given that these are generally not known in

astrophysical applications, the prudent course is to apply each test and note if any of them give results highly discrepant from the rest. See Feigelson & Nelson (1985) and references therein for a more complete description of these techniques.

3.3.1 H I data

The Kaplan–Meier estimator of the full H I dataset ($N = 252$) is shown in Fig. 4. The mean value for the distribution is

$$\overline{\log(f_{\rm H\,I}/f_B)} = -9.282 \pm 0.060. \quad (8)$$

For the barred ($N_B = 72$) and nonbarred ($N_A = 180$) samples, shown in Fig. 5(a), the results are

$$\overline{\log(f_{\rm H\,I}/f_B)_B} = -9.191 \pm 0.103 \quad (9a)$$

and

$$\overline{\log(f_{\rm H\,I}/f_B)_A} = -9.320 \pm 0.074. \quad (9b)$$

These values are just barely consistent with each other at the 1σ level. The two-sample tests were applied to these samples, with the result that the null hypothesis that the two samples are drawn from the same parent population is supported with a probability of between $P = 0.26$ for the logrank test, and $P = 0.51$ for the Gehan test. The logrank test applies equal weights to the censored values. The Gehan test defines the weight for a given limit based on the number of detections with larger values than limit. The presence or absence of (recognized) bars is not significantly correlated with the relative H I content of S0 galaxies in this sample.

This analysis was repeated, using the S0 ($N_0 = 199$) vs S0/*a* ($N_a = 53$) samples. The distributions from the Kaplan–Meier estimator are shown in Fig. 5(b), from which mean values of

$$\overline{\log(f_{\rm H\,I}/f_B)_0} = -9.441 \pm 0.065 \quad (10a)$$

and

$$\overline{\log(f_{\rm H\,I}/f_B)_a} = -8.607 \pm 0.073. \quad (10b)$$

have been derived. These values are discrepant to many σ. Recourse to the two-sample tests reinforces this conclusion, as they all give probabilities that the null hypothesis is upheld of $P < 10^{-4}$. Thus, we reach the same conclusion as did Wardle & Knapp (1986): the H I content of S0/*a* galaxies is significantly higher, on average, than that of "pure" S0 galaxies. In fact, Wardle and Knapp concluded that the distribution function of the H I content of S0's is indistinguishable from that of E's, while the distribution function of S0/*a*'s closely resembles that of Sa's. They interpret this to imply that, in general, any H I gas in S0 systems has been obtained via accretion, while the H I gas in S0/*a* systems is intrinsic (either primordial or reprocessed gas).

3.3.2 FIR data

The Kaplan–Meier distribution for the relative FIR emission of the full dataset is shown in Fig. 6. The resulting mean value is

$$\overline{\log(f_{\rm FIR}/f_B)} = -0.875 \pm 0.054 \quad (11)$$

The distributions for the barred versus unbarred subsamples are shown in Fig. 7(a). The mean values are

$$\overline{\log(f_{\rm FIR}/f_B)_B} = -0.788 \pm 0.098 \quad (12a)$$

and

$$\overline{\log(f_{\rm FIR}/f_B)_A} = -0.911 \pm 0.065. \quad (12b)$$

These values differ by roughly the sum of their variances. The two-sample tests all support the null hypothesis with $P = 0.29$ for the Gehan test, up to $P = 0.42$ for the Cox–Mantel test (a *k*-sample test, similar to the logrank test). Thus, as is the case for relative H I content, the presence or absence of bars in this sample does not significantly affect the relative FIR emission.

For the S0 vs S0/*a* samples, the Kaplan–Meier distributions are shown in Fig. 7(b). The mean values are

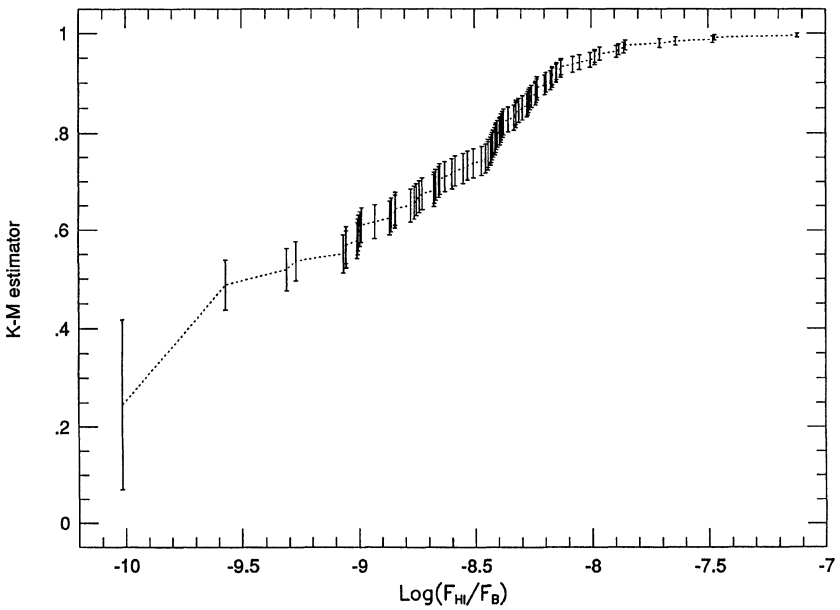

FIG. 4. Kaplan–Meier distribution of relative H I content for the full sample. Error bars are 1σ in this and all subsequent Kaplan–Meier distribution plots.

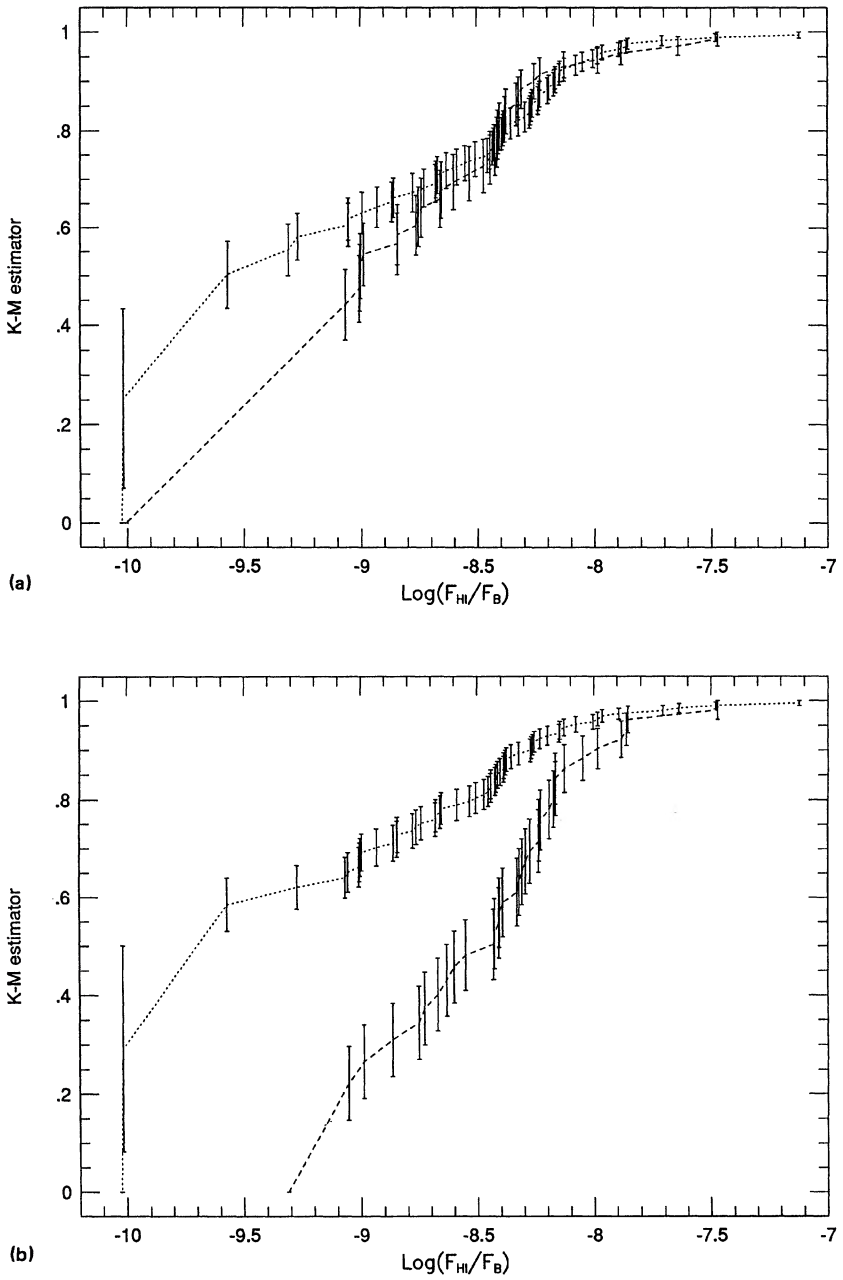

FIG. 5. Kaplan–Meier distributions of the H I content for the morphologically distinct subsets: (a) nonbarred (dotted line) vs barred (dashed line) galaxies; (b) S0 (dotted line) vs S0/*a* (dashed line) galaxies.

$$\overline{\log(f_{\rm FIR}/f_B)_0} = -0.985 \pm 0.061 \quad (13a)$$

and

$$\overline{\log(f_{\rm FIR}/f_B)_a} = -0.415 \pm 0.096. \quad (13b)$$

As in the case of the H I data, these values are formally distinct to many σ. The two-sample tests further confirm that the samples are distinct, with $P \leqslant 10^{-4}$ for all tests. Consistent with the results for the linear regressions given above, the S0/*a* galaxies exhibit a much stronger relative FIR emission that do the S0 galaxies. This will be discussed further below.

3.3.3 $r_{60/100}$

The ratio of the 60–100 μm fluxes ($r_{60/100}$) is typically viewed as a rough estimate of the dust temperature (see, e.g., Low *et al.* 1984). We computed this quantity from the 60 and 100 μm fluxes given in KGKJ. For those systems with upper limits in 60 μm, but detections in 100 μm, it is possible to obtain only an upper limit to $r_{60/100}$. For those with 60 μm fluxes, but 100 μm limits, one can compute only a lower limit on $r_{60/100}$. For those with double limits, the quantity $r_{60/100}$ is undefined. Therefore, the full samples of 252 systems is reduced in the following analysis to 175 systems with at least

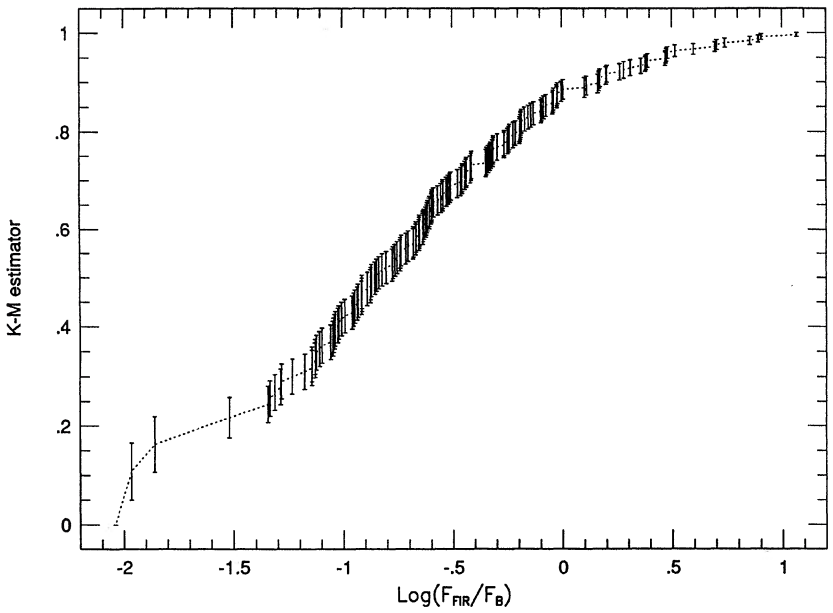

FIG. 6. Kaplan–Meier distribution of the relative FIR emission for the full sample.

one detection in the two *IRAS* FIR bands.

As the FIR and 21 cm line fluxes are probes of different components of the ISM in galaxies (the warm dust and the neutral hydrogen), one would expect, to first order, that $r_{60/100}$ would not correlate strongly with the relative H I content. These data are shown in Fig. 8. As expected, no strong correlation is apparent. The Kendall's τ test gives only a 14% probability that the two variables are statistically correlated. The mean value of $r_{60/100}$ from the Kaplan–Meier estimator is 0.408 ± 0.018, irrespective of H I content. There are a few seriously discrepant points ($r_{60/100} > 0.8$, see Table 3). Removing these gives a mean of 0.373 ± 0.014. All subsets (barred, nonbarred, S0, S0/*a*) give results consistent with this.

Removing the systems with known nuclear emission leaves us a set of 150 objects with definable values or limits for $r_{60/100}$. The Kendall's τ test gives a slightly higher probability that $r_{60/100}$ is correlated with H I content for this sample ($P \approx 0.18$). However, the mean from the Kaplan–Meier estimator, $\overline{r_{60/100}} = 0.397 \pm 0.020$, provides quite a reasonable fit to the data, and is well within 1σ of the result obtained with the full dataset (see Fig. 8). Therefore, our results do not indicate any significant effect on $r_{60/100}$ due to the presence of AGN in our sample.

As discussed above, $r_{60/100}$ appears not to be a function of either galaxy morphology or H I content. It does appear to be a weak function of relative FIR emission (see Fig. 9), with a power-law slope of only ≈ 0.14, but the significance of this is questionable. This is in distinct contrast to the rather steep correlation found by Soifer *et al.* (1987) for a sample of FIR-bright galaxies. The mean relative FIR emission of their sample is, however, approximately 1.5 dex higher than ours. It is hardly surprising that qualitative changes in the relationship between relative amount of FIR and the temperature of the emitting material could take place over such a range in relative emission. Our sample, both with and without the high $r_{60/100}$ points (see Table 3 and above), was split into the S0 vs S0/*a*, and barred versus nonbarred subsamples. These subsamples were analyzed with the two-sample tests, and in all cases the null hypothesis is upheld: the presence or absence of bars, and the differences between S0 and S0/*a* systems do not affect the distribution function of $r_{60/100}$.

Figure 10 shows a histogram of the $r_{60/100}$ values. The mean values of the sample both with and without the highly discrepant points are shown. Also shown is the value $r_{60/100\,c} = 0.447$ which Helou (1986) argues is a rough separation point for objects from which most of the FIR emission is due to current star formation ($r_{60/100} \geqslant r_{60/100_c}$) and those objects with FIR color indistinguishable from Galactic cirrus. This issue is also discussed in Thronson & Bally (1987). For our sample, 60 of 175 (roughly 34%) of the galaxies lie above the critical value of Helou.

4. DISCUSSION

4.1 The Role of Nuclear Emission

As noted in Sec. 3, for a variety of the tests performed, those galaxies which are known to possess a nuclear nonthermal continuum source (see Table 2) were removed from the sample. In all cases, the removal of these objects did not produce a significant change in the results obtained. However, there are two possible reasons for this that can be investigated rather simply. First, the small number of systems with known nuclear emission could lead to them not having a statistically significant effect on the total sample, even if they themselves are drawn from a statistically different parent population than are the normal galaxies. Second, there could be a large number of systems in the "normal" galaxy sample which actually possess unrecognized or even hidden (from optical probes) nuclear sources. In order to investigate these possibilities, we have analyzed the samples of normal and active galaxies with the statistical techniques used

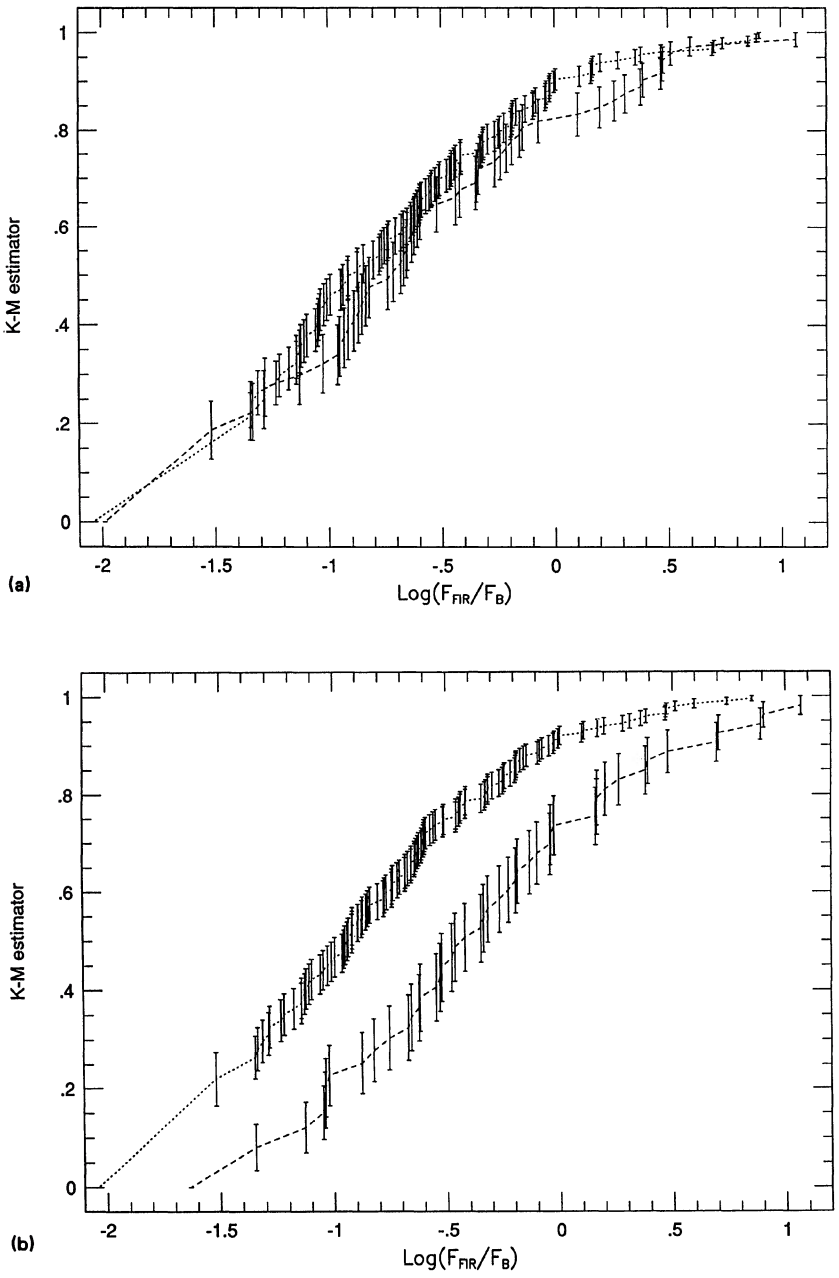

FIG. 7. Kaplan–Meier distributions of the FIR emission for the morphologically distinct subsets: (a) nonbarred (dotted line) vs barred (dashed line) galaxies; (b) S0 (dotted line) vs S0/*a* (dashed line) galaxies.

above. As noted in Sec. *3.3*, the mean value of the relative H I content of the full data sample is $\overline{\log(f_{\rm H\,I}/f_B)} = -9.282 \pm 0.060$. When the sample is split into normal ($N = 227$) and active ($N = 25$) galaxy subsets, the Kaplan–Meier estimator gives

$$\overline{\log(f_{\rm H\,I}/f_B)_n} = -9.347 \pm 0.062 \qquad (14a)$$

and

$$\overline{\log(f_{\rm H\,I}/f_B)_a} = -8.567 \pm 0.097. \qquad (14b)$$

These values are formally distinct to many σ. The distribution functions for the two samples are shown in Fig. 11(a). Note that, although the normal galaxy result is within 1σ of the value for the full dataset, the value for the active galaxies is discrepant by many σ. The two-sample tests confirm this, all giving $P \leqslant 10^{-3}$ that the two samples are drawn from the same parent population. The physical content of this is that the S0 galaxies in our sample with active nuclei have a statistically significantly higher relative H I content than do the S0 galaxies in our sample without active nuclei. It may be that the presence of an active nucleus may be more a function of the presence of a fuel supply than of a central engine.

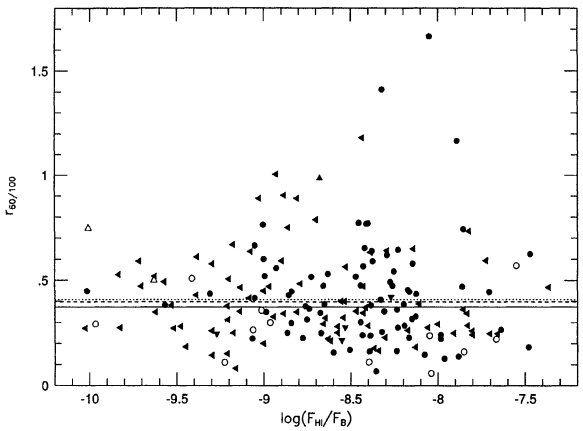

FIG. 8. $r_{60/100}$ vs $\log(F_{\rm H\,I}/F_B)$ for all galaxies with at least one detected FIR band. Full circles are 60 and 100 μm, and H I detections. Left-pointing solid triangles are 60 and 100 μm detections, but H I upper limits. Upward-pointing solid triangles are 60 μm and H I detections, but 100 μm upper limits. Downward-pointing triangles are 100 μm and H I detections, but 60 μm upper limits. Upward-pointing open triangles are 60 μm detections, but 100 μm and H I upper limits. Open circles are 100 μm detections, but 60 μm and H I upper limits. The mean value for the full sample is given by the dotted line. The solid line gives the mean value for those galaxies with $r_{60/100} < 0.8$. The dashed line gives the mean value for the data with the AGN removed.

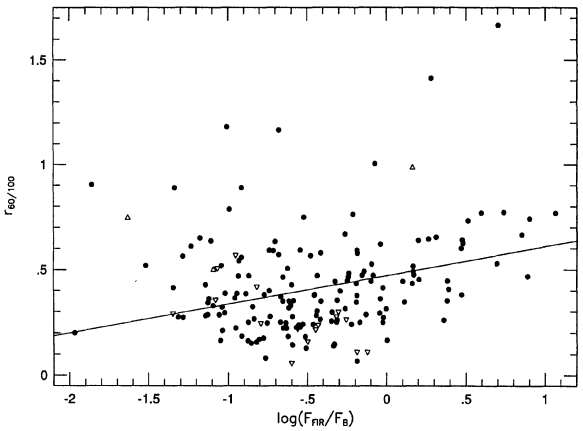

FIG. 9. $r_{60/100}$ vs $\log(F_{\rm FIR}/F_B)$ for all galaxies with at least one good FIR-band measurement. Solid dots are both 60 and 100 μm detections. Upward- and downward-pointing symbols are for 100 and 60 μm limits, respectively. The line is the best-fit linear regression using Schmitt's method.

Alternatively, it may be, as suggested by Byrd *et al.* (1987), that nuclear activity in early type galaxies is triggered by an accretion event, which would cause the increase we see in the relative amount of ISM in these galaxies. In order to address these possibilities more fully, one would have to construct volume limited samples of S0's with and without AGN, then obtain H I 21 cm measurements of these samples down to some consistent limit. We can make no strong statement on the possibility raised above in the absence of such data, as it is unclear to what extent selection effects on our small sample of AGN may influence our result. However, it is difficult to see how any such selection effect could be differential. That is, how it could preferentially give us higher relative H I content for S0's with AGN as opposed to normal S0's.

It is well known that active nuclei emit in the FIR, therefore, we would expect the relative FIR emission from S0's with active nuclei to be greater than that from normal S0's.

TABLE 3. Galaxies with anomalously large $r_{60/100}$.

Name	$r_{60/100}$	HI/FIR area
NGC 315	0.889	On fit line
NGC 984	1.167	HI-Rich
UGC 3426	1.412	On fit line
NGC 2950	0.889	fit/HI-rich
NGC 3419	> 0.986	On fit line
NGC 3516	1.005	fit/HI-poor
NGC 4008	1.182	HI-Rich
NGC 4958	0.903	On fit line
IC 5063	1.666	On fit line

From Sec. *3.3*, the result for the full dataset was -0.875 ± 0.054. For the normal and active galaxy subsets the results are

$$\overline{\log(f_{\rm FIR}/f_B)_n} = -0.948 \pm 0.058 \quad (15a)$$

and

$$\overline{\log(f_{\rm FIR}/f_B)_a} = -0.319 \pm 0.118. \quad (15b)$$

The distribution functions are shown in Fig. 11(b). In order to attach a numerical probability to the obvious, we analyzed these samples with the two-sample tests. All tests gave $P \leqslant 2 \times 10^{-4}$ that the samples are drawn from the same parent population. As expected, active S0's have a much higher rate of relative FIR emission than do normal S0's.

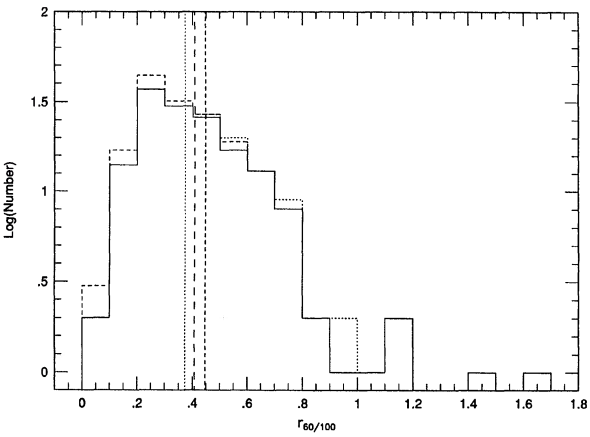

FIG. 10. Histogram of $r_{60/100}$ values. The solid histogram is derived from galaxies detected in both 60 and 100 μm. The dashed portions include those systems with upper limits to $r_{60/100}$. The dotted portions include also the systems with lower limits. The long-dashed line is the mean for the full dataset. The dotted line is the mean for the data with $r_{60/100} < 0.8$. The short-dashed line is the discriminant line proposed by Helou (1986).

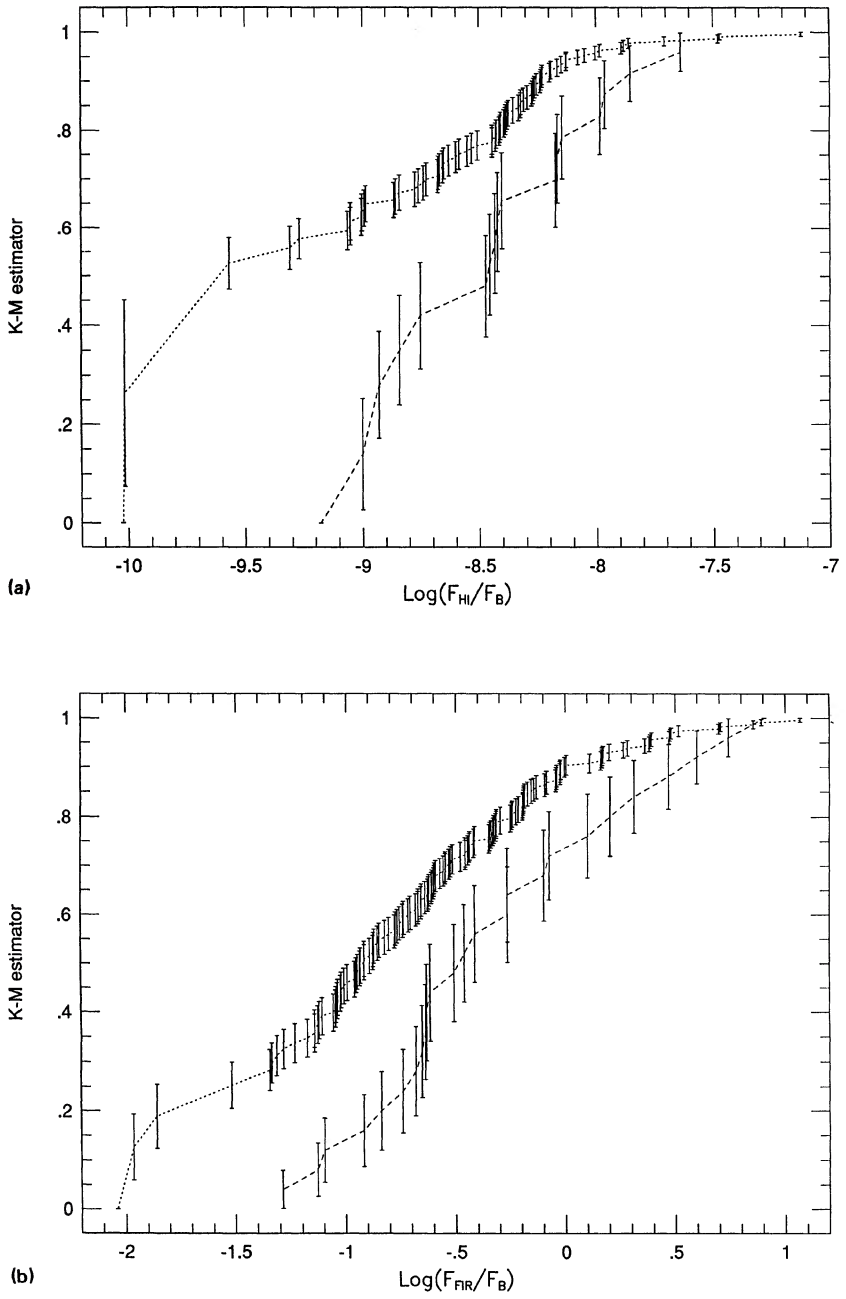

FIG. 11. Kaplan–Meier distributions for the systems with (dashed lines) and without (dotted lines) known nuclear emission: (a) distributions of relative H I content; (b) distributions of relative FIR emission.

Finally, we examined the effect on $r_{60/100}$ of the presence or absence of active nuclei in our sample. From Sec. *3.3*, $\overline{r_{60/100}} = 0.408 \pm 0.018$. For the normal and active galaxy samples the results are

$$\overline{r_{60/100_n}} = 0.397 \pm 0.020 \quad (16a)$$

and

$$\overline{r_{60/100_a}} = 0.471 \pm 0.043. \quad (16b)$$

These values are discrepant at $> 2\sigma$, in the sense that the S0 galaxies with AGN have larger 60–100 μm flux ratios. The two-sample tests indicate that this difference is probably significant; the probability that the null hypothesis is upheld is $0.066 \leqslant P \leqslant 0.093$ depending on which test is used.

The values for $r_{60/100}$ given above correspond to spectral indices of $\alpha_n = -1.81 \pm 0.10$ and $\alpha_a = -1.47 \pm 0.18$, where $f_\nu \propto \nu^\alpha$. In contrast, Miley *et al.* (1985) find $\alpha \sim -0.9$ for a sample of AGN (Seyfert 1, Seyfert 2, and H II galaxies) drawn from Veron-Cetty & Veron (1984). Our result is, however, in complete agreement with that of Goodrich (1989), who found $\alpha \approx -1.46$ for a small sample of Seyfert 1.8 and 1.9 galaxies. The average value of $r_{60/100}$ for the sample of bright, normal, early type disk galaxies (S0

through Sb, including both barred and nonbarred systems) reported by de Jong *et al.* (1984) is consistent with our results. Converting from their notation, we derive $\overline{r_{60/100_{dJ}}} \approx 0.38 \pm 0.04$. The sample of S0 and SB0 galaxies from de Jong *et al.* gives a somewhat higher result than this, but contains only six galaxies. This difference is therefore not statistically significant.

4.2 The Relationship of H I content to FIR emission

We now consider the physical underpinnings of the relationship between the relative H I content and FIR emission in S0 galaxies. First, it is clear that there is no simple physical correlation between the two quantities for our sample. There is a statistical correlation, which one can make various physical arguments to explain. What we have done is to examine the data for two tracers of different components of the ISM is S0 galaxies, scaled by total starlight. Thus, the statistical correlation we see tells us the following: S0 galaxies with large H I components (per unit starlight) also tend to have large FIR emitting components (again, per unit starlight), and *vice versa*. That is, the ISM in S0 galaxies is a normal ISM on the galactic scale—both components are present, in roughly similar proportions for a given morphological type. Clearly, there are strong exceptions to this that are discussed further below. The bulge dynamics do not appear to influence this correlation, as the presence or absence of recognized bars is not a statistically significant factor. Inspection of Figs. 2(a), 2(b), 5(a), and 7(a) reveals that this conclusion is unlikely to be altered if the "nonbarred" sample is, in fact, contaminated by galaxies with weak or infrared bars. The S0/*a* sample appears to show a steeper correlation than does the S0 sample. This suggests that there is more of whatever generates FIR—per unit H I—in the ISM of S0/*a* galaxies than in that of S0 galaxies. Assuming the bootstrap to give reasonable estimates for the errors for the fit parameters from Schmitt's method, this effect is present at the $\approx$96% confidence level.

Our comparison of the H I content and FIR emission of the various morphological subsets indicates that, once again, the bulge dynamics do not significantly affect either $F_{\rm H\,I}/F_B$ or $F_{\rm FIR}/F_B$. Neither morphology nor H I content appears to affect $r_{60/100}$. It may correlate with $F_{\rm FIR}/F_B$, in the sense that more total $F_{\rm FIR}/F_B$ implies a higher $r_{60/100}$, but any such correlation is quite weak. However, the S0 galaxies have less H I per unit starlight than the S0/*a*'s (as shown by Wardle & Knapp 1986), as well as less FIR per unit starlight. One could interpret this last as an indication that S0/*a* galaxies tend to have more current star formation than do S0's. Alternatively, it may simply be that S0/*a*'s have a more extensive diffuse ISM than do S0's. Several recent studies of later-type disk galaxies indicate that substantial amounts of FIR flux come from regions which are spatially distinct from either resolved regions of massive star formation or strong CO sources (Jackson *et al.* 1991; Smith *et al.* 1991; see also Disney *et al.* 1989). It may thus be that, in systems with little massive star formation, such as S0's (*and* S0/*a*'s), that the bulk of the FIR comes from something akin to Galactic cirrus. Another possibility is a significant portion of the FIR originates from regions of exclusively low-mass star formation. There are, however, no good observational tests of this hypothesis at present.

At this point we reconsider the problem mentioned in Sec. *2.1*; the heterogeneity of the H I data. The statistical methods we have used all make simplifying assumptions about the nature of the error bars associated with the data. Inspections of Fig. 1 shows the actual errors to be quite heterogeneous. This is clearly more of a problem for the H I than the FIR data. However, the following observation seems to indicate that our results are not strongly effected by this problem: For those systems detected in H I, the 1σ errors in $F_{\rm H\,I}/F_B$ are not a strong function of $F_{\rm H\,I}/F_B$. The errors for the 20 systems with the highest detected $F_{\rm H\,I}/F_B$ ratios are about twice as large as those for the 20 systems with the lowest detected $F_{\rm H\,I}/F_B$ ratios. We conclude from this that the heterogeneity of the H I data is not likely to invalidate our results.

4.3 Extreme Outliers

Looking back to Fig. 1, one must note that, as discussed above, the relationship between H I content and FIR emission for our sample is not at all clean. The reasons for this have just been discussed. We now turn our attention to the extreme outlying galaxies in the figure. Table 4 lists those systems for which the H I content is much higher than would be expected based on the FIR emission (or upper limit). A number of these systems have been mapped in H I (see Tables 1 and 4). The distribution of H I in those systems that are most strongly deviant suggests that their H I gas has been accreted. The gas lies in outer rings, and is often highly inclined with respect to the optical disk. Also, all of the very deviant objects for which we have Hα maps show no emission down to quite low levels. We infer from these arguments that the majority of the systems in Table 4 have accreted their gas. Subsequent H I mapping of these systems should reveal their H I components to be dynamically distinct from their stellar components. Specifically, this work suggests the H I gas in the following systems is most likely accreted: NGC 936, 984, 1533, 1596, 5084, 5291, 5493, UGC 1353.

Listed in Table 5 are those systems which have anomalously strong FIR emission for their H I content (or upper limit). It is not so clear that there is any single explanation for the location of these systems in Fig. 1. A particularly interesting case is NGC 4710. This galaxy was only very recently detected in H I (Kenney *et al.* 1991). Prior to its detection in H I, it had been detected in CO (Kenney & Young 1988). It is also a clear detection in Hα (Pogge & Eskridge 1991, in preparation). The membership of this galaxy in the Virgo cluster points to a possible explanation of all this: This is an example of an early type spiral system which has been stripped of its neutral gas component via an interaction with the intracluster medium (ICM) of the Virgo cluster. In the absence of detailed H I and CO maps for the other cluster members in Table 5, we speculate that these systems have been stripped of their neutral gas (or had their neutral gas converted into molecular material) by some process resulting from an interaction of their neutral gas components with the ICM. This process may also be responsible for triggering episodes of star formation in the molecular clouds deep in the potentials of these systems. We would thus expect deep Hα imaging to reveal nuclear and circumnuclear star formation regions in many of these systems. Those systems that are not members of rich clusters may also be undergoing a burst of star formation due either to interactions with companions, or to internal processes. If this is the case, we expect that any such star formation would be much less confined to the nuclear regions than in the case of the cluster systems.

TABLE 4. Galaxies with anomalously large H I flux.

Name	Type	21cm flux Jykm/sec	σ_{HI} Jykm/sec	FIR flux 10^{-14} W/m^2	σ_{FIR} [a] 10^{-14} W/m^2	Notes†
NGC 148	0	10.70	1.52	0	2.29	
NGC 160	1	8.72	1.06	2.60	0.54	
NGC 680	0	4.00	0.84	0	1.85	j)
UGC 1353	0	10.60	4.09	2.64	0.38	
NGC 936	0B	6.00	2.00	0	1.67	j)
NGC 984	0	7.80	0.42	1.31	0.55	
NGC 1023	0B	63.00	3.60	0	1.73	j) l)
NGC 1167	0	11.51	1.23	3.38	0.56	
NGC 1302	1	20.30	3.49	3.19	0.25	
IC 2006	0	3.00	0.17	1.61	0.22	b) SVS
NGC 1533	0B	87.50	28.64	5.71	0.41	
NGC 1596	0	15.70	9.30	0	1.25	
NGC 2685	0p	32.30	1.74	7.14	0.57	h) l)
NGC 2787	0B	15.30	2.29	7.23	0.87	l)
NGC 2962	0B	10.26	0.83	3.53	0.55	
NGC 3900	1	17.60	1.33	7.60	0.72	l)
NGC 4203	0	27.20	1.50	9.54	0.41	e) l) m)
NGC 4262	0B	10.60	0.89	2.29	0.55	l)
NGC 4866	1	22.16	0.76	3.54	0.76	
NGC 5084	0	96.40	43.03	9.24	1.20	l)
NGC 5101	1B	57.26	2.64	20.78	0.98	l)
NGC 5102	0	72.00	6.99	13.26	0.49	l)
NGC 5291	0	63.00	9.45	0	1.85	
NGC 5493	0	8.00	2.60	0	1.62	
NGC 5820	0	6.80	4.95	1.01	0.31	
UGC 10528	0	5.70	0.50	0	1.67	
NGC 6501	1	5.20	0.64	0	2.14	j) l)

a). The values listed for upper limit points are $3\sigma_{FIR}$.
†). See notes to Table I.

From Fig. 8, there are a number of objects with values of $r_{60/100}$ very much larger than the mean value ($\approx$0.4). There are nine systems with values larger than 0.8 (see Table 3). Five of these nine (NGC 315, 3419, 4958, IC 5063, UGC 3426) fall on the fit line for H I content versus FIR emission. Three are on the H I-rich side of the line (NGC 984, 2950, and 4008), two significantly so (NGC 984 and 4008). The last (NGC 3516) is somewhat H I-poor its FIR emission, but is also a strong Seyfert 1 galaxy (Seyfert 1943). If we infer from the high values of $r_{60/100}$ that the FIR emission from these galaxies is largely due to dust heated by vigorous current star formation, this leads us to conclude that the relative contribution of star formation activity to the production of FIR emission in S0 galaxies is effectively independent of any FIR versus H I correlation. Those galaxies with the highest values of $r_{60/100}$, and, therefore, the highest dust temperatures do not have excessively large amounts of FIR relative to their stellar continua.

5. SUMMARY AND CONCLUSIONS

We have examined the relationship between H I content and FIR emission for a sample of 252 early type disk galaxies (type S0, SB0, S0/*a*, SB0/*a*). Due to the presence of upper limits, we have used the techniques of survival analysis (see Schmitt 1985, Feigelson & Nelson 1985, and Isobe *et al.* 1986) to address our data. We find a clear indication that relative H I content and FIR emission are statistically correlated in our sample. Performing a linear regression on the logarithms of these quantities yields a slope of essentially unity. This result is not significantly effected by bulge dynamics, as the analysis of subsamples of barred and nonbarred systems yield the same result. Disk dynamics may be significant, however, as the slope of the regression for the S0 sample is shallower than that for the S0/*a* sample at the 98.5% confidence level. Removing the known AGN from our sample reduces the significance to the $\approx$96% confidence level.

We have studied the distribution functions of our data using the Kaplan–Meier estimator and a variety of two-sample tests (Feigelson & Nelson 1985). Once again, the bulge dynamics do not have a statistically significant effect on the relative H I content or FIR emission of our sample. The disk dynamics do, as the S0/*a* sample has both a higher relative H I content and stronger relative FIR emission than does the S0 sample. So, although the bulge dynamics do not appear to influence the H I FIR correlation, the disk dynamics do affect it in the sense that there is more material emitting in the FIR per unit H I in the S0/*a* sample than in the S0 sample. It may be that this is due to more vigorous current star formation in S0/*a* galaxies than in S0's. Or it may simply be that S0/*a*'s have a more extensive diffuse ISM than do S0's.

As expected, there is no strong correlation between H I content and $r_{60/100}$. There may be a correlation between FIR emission and $r_{60/100}$, but it is quite weak, if present at all. This finding differs from that of Soifer *et al.* (1987), who found a correlation with quite a steep slope. Their sample was, how-

TABLE 5. Galaxies with anomalously large FIR.

Name	Type	21cm flux Jykm/sec	σ_{HI} a) Jykm/sec	FIR flux 10^{-14} W/m^2	σ_{FIR} 10^{-14} W/m^2	Notes†
IC 89	0B	2.28	0.71	20.67	0.66	
NGC 632	0	3.30	0.56	53.20	0.75	
UGC 1385	1B	2.10	0.59	64.93	0.39	
NGC 1400	0	0	1.34	13.33	0.63	
NGC 1819	0B	2.80	0.97	85.28	0.47	g)
NGC 3245	0	0	0.70	24.36	0.49	f)
NGC 3516	0B	0	2.50	18.54	0.74	
NGC 3593	1	10.49	0.56	230.10	0.40	g) o)
NGC 4124	0	0	0.66	7.36	0.47	
NGC 4150	0	0	0.27	15.27	0.41	
NGC 4293	1	0	3.50	46.69	0.52	
NGC 4310	0	2.13	0.43	13.44	0.52	n)
NGC 4385	0B	4.68	1.25	48.18	0.46	i)
NGC 4429	0	0	1.43	23.77	0.58	n)
NGC 4435	0B	0	0.93	25.80	0.60	d) n)
NGC 4451	0	3.36	0.40	24.88	0.52	n)
NGC 4457	1	7.40	1.11	59.77	0.45	g)
NGC 4476	0	0	0.78	9.27	0.53	
NGC 4526	0	0	0.94	97.62	1.07	f) h)
NGC 4710	0	0.32	0.04	77.39	0.72	d) g) q)
NGC 5273	0	0	1.22	10.35	0.54	
NGC 5363	0	1.80	0.50	24.12	0.45	e) h)
NGC 5866	0	0	5.00	82.04	0.29	g)
IC 5063	1	9.70	1.76	56.70	0.77	
NGC 7252	0p	0	8.20	49.75	0.40	
NGC 7625	1	19.58	0.61	113.80	0.42	g)
NGC 7648	0	0.66	0.22	54.86	0.56	
NGC 7679	1	14.12	1.57	83.53	0.57	

a). The values listed for upper limit points are $3\sigma_{HI}$.
†). See notes to Table I.

ever, qualitatively very different from ours: Those systems in our sample with the strongest relative FIR emission are approaching the median value for the sample of Soifer *et al.* It would seem that below a threshold level of $\log(f_{FIR}/f_B) \sim 0.5$ the relative strength of the FIR emission becomes largely decoupled from $r_{60/100}$. The mean value for $r_{60/100}$ in our sample is ~ 0.4. This value is not significantly different for any of the morphological subsamples, nor is it altered by the removal of the known AGN. The AGN alone do, however, have a higher mean $r_{60/100}$ value at the 2σ level. Roughly 34% of our sample have $r_{60/100}$ above the critical value of 0.447 proposed by Helou (1986) as a demarcation, above which a majority of the FIR is expected to be due to star formation.

We examined the relative H I content and FIR emission of our sample of known AGN versus the remainder (presumed non-AGN), and found the AGN to have stronger relative FIR emission, as expected. We also found the AGN to have higher relative H I content than the non-AGN at the $\sim 7\sigma$ level. Possible interpretations of this are that the presence of a central engine is ubiquitous, and only those galaxies with sufficient ISM can exhibit AGN, or that nuclear activity in early type galaxies is triggered by an accretion event that also supplies the excess H I we see. To address this issue properly would require H I 21 cm line data to some low, consistent flux level for statistically complete, volume limited samples of S0's with and without AGN.

The fundamental conclusion of this study is that S0 galaxies have a normal ISM: Those with proportionally more H I tend also to have proportionally more FIR and *vice versa*. A straightforward prediction of this is that, when sufficiently large samples of S0's have been observed in tracers of other components of the ISM (e.g., CO line emission, Hα line emission, x rays) the general correlation we find will hold up: Systems with more of one component (per unit starlight) will have more of all other components on average.

There are a number of galaxies that deviate strongly from the trends we find. Based on H I synthesis maps of a number of the systems with excess H I, we predict that many of the following galaxies are likely to have H I morphologies indicative of gas accretion: NGC 936, 984, 1533, 1596, 5084, 5291, and 5493, and UGC 1353. Those systems with excess FIR emission are, in many cases, members of rich clusters. Observations of one of these galaxies in particular (NGC 4710) lead us to conclude that these systems have lost much of their neutral gas via interactions with the ICM of their parent cluster. Other objects, not part of rich clusters, may be currently undergoing short-lived bursts of enhanced star

formation. Detailed observations of these galaxies in CO, Hα, and FIR are required to further investigate this possibility.

We would like to thank Dr. G. Knapp for kindly providing us with the coadded *IRAS* data for early type galaxies in advance of its publication, and Dr. E. Feigelson and M. LaValley for providing us with a copy of ASURV, a software package for survival analysis, and for several very useful discussions of statistical methods. We would also like to thank the referee for a careful reading of the original text and two excellent suggestions that significantly strengthened the analysis in this paper. P. E. would also like to thank the Astronomy Department at Columbia University for asking good questions, and Michael Kearney of the David Rittenhouse Computing facility for his help with some painful software problems. This research was partially supported by funds from the Margaret Cullinan Wray Charitable Lead Annuity Trust.

REFERENCES

Balick, B., Faber, S. M., and Gallagher, J. S. 1976, ApJ, 209, 710
Balkowski, C., and Chamaraux, P. 1983, A&AS, 51, 331
Bally, J., and Thronson, Jr., H. A. 1989, AJ, 97, 69
Bieging, J. H., and Biermann, P. 1977, A&A, 60, 361
Burstein, D., and Heiles, C. 1984, ApJS, 54, 33
Byrd, G. G., Sundelius, B., and Valtonen, M. 1987, A&A, 171, 16
Chamaraux, P., Balkowski, C., and Fontanelli, P. 1986, A&A, 165, 15
de Jong, T., Clegg, P. E., Soifer, B. T., Rowan-Robinson, M., Habing, H. J., Houck, J. R., Aumann, H. H., and Raimond, E. 1984, ApJ, 278, L67
de Vaucouleurs, G., de Vaucouleurs, A. and Corwin, H. G. 1976, Second Reference Catalog of Bright Galaxies (University of Texas Press, Austin) (RC2)
Disney, M., Davies, J., and Phillips, S. 1989, MNRAS, 239, 939
Feigelson, E. D., and Nelson, P. I. 1985, ApJ, 293, 192
Giovanardi, C., Krumm, N., and Salpeter, E. E. 1983, AJ, 88, 1719
Goodrich, R. W. 1989, ApJ, 340, 190
Haynes, M. P., Herter, T., Barton, A. S., and Benensohn, J. S. 1990, AJ, 99, 1740
Helou, C. 1986, ApJ, 311, L33
Hubble, E. 1936, The Realm of the Nebulae (Yale University Press, New Haven), p. 36
Huchra, J. 1983, private communication
Huchtmeier, W. K. 1982, A&A, 110, 121
Hunter, D. A., Thronson, Jr., H. A., Casey, S., and Harper, D. A. 1989, ApJ, 341, 697
Isobe, T., Feigelson, E. D., and Nelson, P. I. 1986, ApJ, 306, 490
Jackson, J. M., Eckart, A., Cameron, M., Wild, W., Ho, P. T. P., Pogge, R. W., and Harris, A. I. 1991, ApJ, 373 (in press)
Kenney, J., and Young, J. S. 1988, ApJS, 66, 261
Kenney, J. D. P., Young, J. S., Rubin, V. C., and Ford, W. K., Jr. 1991, in preparation
Knapp, G. R., Turner, E. L., and Cunniffe, P. E. 1985, AJ, 90, 454
Knapp, G. R., Guhathakurta, P, Kim, D. -W., and Jura, M. 1989, ApJS, 70, 329 (KGKJ)
Lonsdale, C. J., Helou, G., Good, J. C., and Rice, W. 1985, Cataloged Galaxies and Quasars in the *IRAS* Survey (Jet Propulsion Laboratory, Pasadena)
Low, F. J., Beintema, D. A., Gautier, T. N., Gillett, F. C., Beichman, C. A., Neugebauer, G., Young, E., Aumann, H. H., Boggess, N., Emerson, J. P., Habing, H. J., Hauser, M. G., Houck, J. R., Rowan-Robinson, M., Soifer, B. T., Walker, R. G., and Wesselius, P. R. 1984, ApJ, 278, L19
Mazzarella, J. M., and Balzano, V. A. 1986, ApJS, 62, 751
Miley, G. K., Neugebauer, G., and Soifer, B. T. 1985, ApJ, 293, L11
Phillips, M. M., Jenkins, C. R., Dopita, M. A., Sadler, E. M., and Binette, L. 1986, AJ, 91, 1062
Pogge, R. W., and Eskridge, P. B. 1987, AJ, 93, 291
Pogge, R. W., and Eskridge, P. B. 1991, in preparation
Sandage, A. 1961, A Hubble Atlas of Galaxies (Carnegie Institute of Washington, Washington, DC), p. 7
Schmitt, J. H. M. M. 1985, ApJ, 293, 178
Schweizer, F., van Gorkom, J. H., and Seitzer, P. 1989, ApJ, 338, 770
Seyfert, C. K. 1943, ApJ, 97, 28
Smith, B. J., Lester, D. F., Harvey, P. M., and Pogge, R. W. 1991, ApJ, 373 (in press)
Soifer, B. T., Sanders, D. B., Madore, B. F., Neugebauer, G., Danielson, G. E., Elias, J. H., Lonsdale, C. J., and Rice, W. L. 1987, ApJ, 320, 238
Thronson, Jr., H. A., and Bally, J. 1987, ApJ, 319, L63
Thronson, Jr., H. A., Tacconi, L., Kenney, J., Greenhouse, M. A., Margulis, M., Tacconi-Garman, L., and Young, J. S. 1989, ApJ, 344, 747
van Driel, W. 1987, Ph.D. dissertation, Groningen University
Veron-Cetty, M. P., and Veron, P. 1984, A Catalogue of Quasars and Active Nuclei (European Southern Observatory, Munich)
Walsh, D. E. P., Knapp, G. R., Wrobel, J. M., and Kim, D.-W. 1989, ApJ, 337, 209
Wardle, M., and Knapp, G. R. 1986, AJ, 91, 23
Zwicky, F., Herzog, E., Wild, P., Karpowicz, M., and Kowal, C. 1960–1968, A Catalog of Galaxies and Clusters of Galaxies (California Institute of Technology, Pasadena)